blood®
Regular Article

IMMUNOBIOLOGY AND IMMUNOTHERAPY

Biallelic *NFATC1* mutations cause an inborn error of immunity with impaired CD8$^+$ T-cell function and perturbed glycolysis

Sevgi Kostel Bal,[1,2] Sarah Giuliani,[1,2] Jana Block,[1-3] Peter Repiscak,[1] Christoph Hafemeister,[1] Tala Shahin,[1-3] Nurhan Kasap,[4,5] Bernhard Ransmayr,[1-3] Yirun Miao,[1-3] Cheryl van de Wetering,[1,3] Alexandra Frohne,[1,2] Raul Jimenez Heredia,[1,2] Michael Schuster,[3] Samaneh Zoghi,[1,2] Vanessa Hertlein,[1-3] Marini Thian,[1-3] Aleksandr Bykov,[1] Royala Babayeva,[4,5] Sevgi Bilgic Eltan,[4,5] Elif Karakoc-Aydiner,[4,5] Lisa E. Shaw,[6] Iftekhar Chowdhury,[7] Markku Varjosalo,[7] Rafael J. Argüello,[8] Matthias Farlik,[6] Ahmet Ozen,[4,5] Edgar Serfling,[9] Loïc Dupré,[2,6,10] Christoph Bock,[2,3,11] Florian Halbritter,[1] J. Thomas Hannich,[3] Irinka Castanon,[1,2] Michael J. Kraakman,[1,2] Safa Baris,[4,5,*] and Kaan Boztug[1-3,12,13,*]

[1]St. Anna Children's Cancer Research Institute, Vienna, Austria; [2]Ludwig Boltzmann Institute for Rare and Undiagnosed Diseases, Vienna, Austria; [3]CeMM Research Center for Molecular Medicine of the Austrian Academy of Sciences, Vienna, Austria; [4]Department of Pediatrics, Division of Allergy and Immunology, Marmara University School of Medicine, Istanbul, Turkey; [5]The Isil Berat Barlan Center for Translational Medicine, Marmara University, Istanbul, Turkey; [6]Department of Dermatology, Medical University of Vienna, Vienna, Austria; [7]Institute of Biotechnology, University of Helsinki, Helsinki, Finland; [8]Aix Marseille University, CNRS, INSERM, CIML, Centre d'Immunologie de Marseille-Luminy, Marseille, France; [9]Department of Molecular Pathology, Institute of Pathology, and Comprehensive Cancer Center Mainfranken, University of Würzburg, Würzburg, Germany; [10]Toulouse Institute for Infectious and Inflammatory Diseases, INSERM, CNRS, Toulouse III Paul Sabatier University, Toulouse, France; [11]Medical University of Vienna, Institute of Artificial Intelligence, Center for Medical Data Science, Vienna, Austria; [12]St. Anna Children's Hospital, Vienna, Austria; and [13]Department of Pediatrics and Adolescent Medicine, Medical University of Vienna, Vienna, Austria

KEY POINTS

- **Germ line biallelic loss-of-function mutations in *NFATC1* underly a previously unknown inborn error of immunity.**
- **NFATc1 defects curtail the activation responses of CD8$^+$ cytotoxic T cells due to impaired glycolysis.**

The nuclear factor of activated T cells (NFAT) family of transcription factors plays central roles in adaptive immunity in murine models; however, their contribution to human immune homeostasis remains poorly defined. In a multigenerational pedigree, we identified 3 patients who carry germ line biallelic missense variants in *NFATC1*, presenting with recurrent infections, hypogammaglobulinemia, and decreased antibody responses. The compound heterozygous *NFATC1* variants identified in these patients caused decreased stability and reduced the binding of DNA and interacting proteins. We observed defects in early activation and proliferation of T and B cells from these patients, amenable to rescue upon genetic reconstitution. Stimulation induced early T-cell activation and proliferation responses were delayed but not lost, reaching that of healthy controls at day 7, indicative of an adaptive capacity of the cells. Assessment of the metabolic capacity of patient T cells revealed that NFATc1 dysfunction rendered T cells unable to engage in glycolysis after stimulation, although oxidative metabolic processes were intact. We hypothesized that NFATc1-mutant T cells could compensate for the energy deficit due to defective glycolysis by using enhanced lipid metabolism as an adaptation, leading to a delayed, but not lost, activation responses. Indeed, we observed increased ^{13}C-labeled palmitate incorporation into citrate, indicating higher fatty acid oxidation, and we demonstrated that metformin and rosiglitazone improved patient T-cell effector functions. Collectively, enabled by our molecular dissection of the consequences of loss-of-function *NFATC1* mutations and extending the role of NFATc1 in human immunity beyond receptor signaling, we provide evidence of metabolic plasticity in the context of impaired glycolysis observed in patient T cells, alleviating delayed effector responses.

Introduction

T cells can have a diverse spectrum of functional states, governed primarily by cues in their environment. Hence, T cells constantly fine-tune their behavior through coordination between signal transduction pathways, gene expression, and cellular metabolism. Studying how metabolic circuitries contribute to T-cell responses is fundamental to our understanding of the immune system and is currently under intense investigation.[1,2] However, most studies have been conducted within the field of chronic inflammation and tumor immunity and typically focus on components within metabolic pathways.

Accordingly, the contribution of transcriptional regulation to metabolic control within T cells, particularly in the context of human disease, remains poorly understood.

The nuclear factor of activated T cells (NFAT) family of transcription factors (TFs) regulates T-lymphocyte activation, survival, proliferation, and differentiation as well as the transcription of many growth factors, cytokines, and cell-to-cell interaction molecules that are essential for the morphogenesis, development, and function of numerous cell types and organ systems.[3-5] The NFAT family comprises 5 members, of which NFATc1, NFATc2, and NFATc3 are strongly expressed in lymphocytes.[5] In T and B cells, stimulation of the antigen receptor (T-cell receptor [TCR] and B-cell receptor, respectively) triggers signaling cascades resulting in Ca^{2+} release from the endoplasmic reticulum to the cytosol. Decreased Ca^{2+} in the endoplasmic reticulum lumen is sensed by stromal interaction molecules that activate pore-forming ORAI proteins at the plasma membrane and induce store-operated Ca^{2+} entry (SOCE).[5-7] Increased cytoplasmic Ca^{2+} leads to the activation of calcineurin, which subsequently dephosphorylates NFATc.[5] Upon dephosphorylation, cytoplasmic NFATc translocates to the nucleus, where it regulates gene transcription in cooperation with various other TFs such as AP-1, a heterodimer consisting of Jun and Fos members.[5-7]

Distinct roles of individual NFATc members have been shown in murine T lymphocytes, particularly during differentiation of T-helper 17 cells (Th17s), T-follicular helper cells (TfHs), and regulatory T cells (Tregs).[3] Perturbations in NFATc activity, due to the loss of the ability to bind to AP-1, are linked to $CD8^+$ T-cell exhaustion upon prolonged stimulation in models of chronic infection and oncogenesis.[8]

Recently, NFATc1 has been discovered as a central regulator of T-cell metabolism. Under physiological conditions, activated $CD8^+$ T cells shift their metabolism from oxidative phosphorylation (OXPHOS) to glycolysis. Dysfunctions of the SOCE/NFAT axis rendered mouse T cells unable to undergo the glycolytic switch necessary for metabolic expenses during activation and clonal expansion.[9,10] Here, we report 2 heterozygous loss-of-function (LOF) mutations in compound heterozygosity in *NFATC1* as the etiology of a previously unknown inborn error of immunity (IEI). We dissect the molecular function of NFATc1 as a TF and extend its role beyond receptor signaling. Specifically, we demonstrate that NFATc1 is required for intact glycolytic metabolism, revealing the fundamental but permissive nature of metabolic circuitries in governing T-cell responses in an IEI setting. In addition, we demonstrate that NFATc1-dysfunctional T cells shift toward using alternative metabolic resources such as fatty acids (FAs), and showcase the exploitability of this phenomenon in patient cells, with the use of metformin and rosiglitazone providing proof-of-concept for therapeutic modulation of immunometabolic states to improve effector functions in a genetically defined T-cell defect.

Material and methods

Study approval

Samples from patients, family members, and other healthy controls (HCs) were obtained after an informed written consent and approval from the ethics committee of Marmara University Faculty of Medicine as well as from the institutional review board of the Medical University of Vienna were obtained.

WES

For whole-exome sequencing (WES), a TrueSeq Rapid Exome kit as well as the Illumina HiSeq3000 system and the cBot cluster generation instruments were used, as previously described.[11] A detailed list of genetic variants is shown in supplemental Tables 2-6, available on the *Blood* website.

Immunoblot experiments

Immunoblots were performed per established protocols, as outlined.[11]

Lymphocyte phenotyping and functions

Cryopreserved peripheral blood mononuclear cells (PBMCs) were stained with fluorescent antibodies (supplemental Table 1). PBMCs or sorted $CD8^+$ T-cell subsets were isolated and cultured in vitro under various conditions,[11] and proliferation, activation, cytokine expression, or apoptosis were determined. Data were acquired with an LSR Fortessa (BD Biosciences) and analyzed using FlowJo version 10. The gating strategies and the panels are shown in supplemental Figure 1 and supplemental Table 1, respectively.

Treatment of T lymphoblasts with metformin and rosiglitazone

Patient and HC T cells were expanded as previously described.[11] Starting on day 5 after the initial stimulation, metformin (2 mM; Sigma), rosiglitazone (1 μM; Sigma), or carrier were added every 2 days until day 10, when the experiments were performed.

Statistical analysis

For individual comparisons of independent groups, the Student *t* test was performed. For multiple comparisons, a one or 2-way analysis of variance was applied, followed by corrections of multiple tests. Analyses were performed using PRISM software (GraphPad Software Inc).

Results

Identification of human *NFATC1* mutations

Here, we studied 3 patients (P1, P2, and P3) from a multigenerational consanguineous pedigree (Figure 1A), who had early-onset sinopulmonary infections requiring multiple hospitalizations and eventually leading to bronchiectasis. In the extended family, we noted that several infants (from whom no genetic material was available for testing) had succumbed to infectious complications (supplemental Information). P2 and P3 experienced recurrent viral (warts) and bacterial (folliculitis and abscesses) skin infections. Thoracolumbal scoliosis, which was corrected by surgery, was documented in P1 and P2 (Figure 1B). Laboratory results indicated hypogammaglobulinemia (more prominently in P1 than in P2 or P3), and low antibody titers after pneumococcus vaccine were detected in P1. P3 had a negative response to hepatitis B vaccine. (supplemental Table 2). Immunophenotyping revealed a lower $CD4^+$:$CD8^+$ T-cell ratio and lower recent thymic emigrants in P1, P2, and P3 compared with age-matched controls. Lymphocyte proliferation responses to phytohemagglutinin and

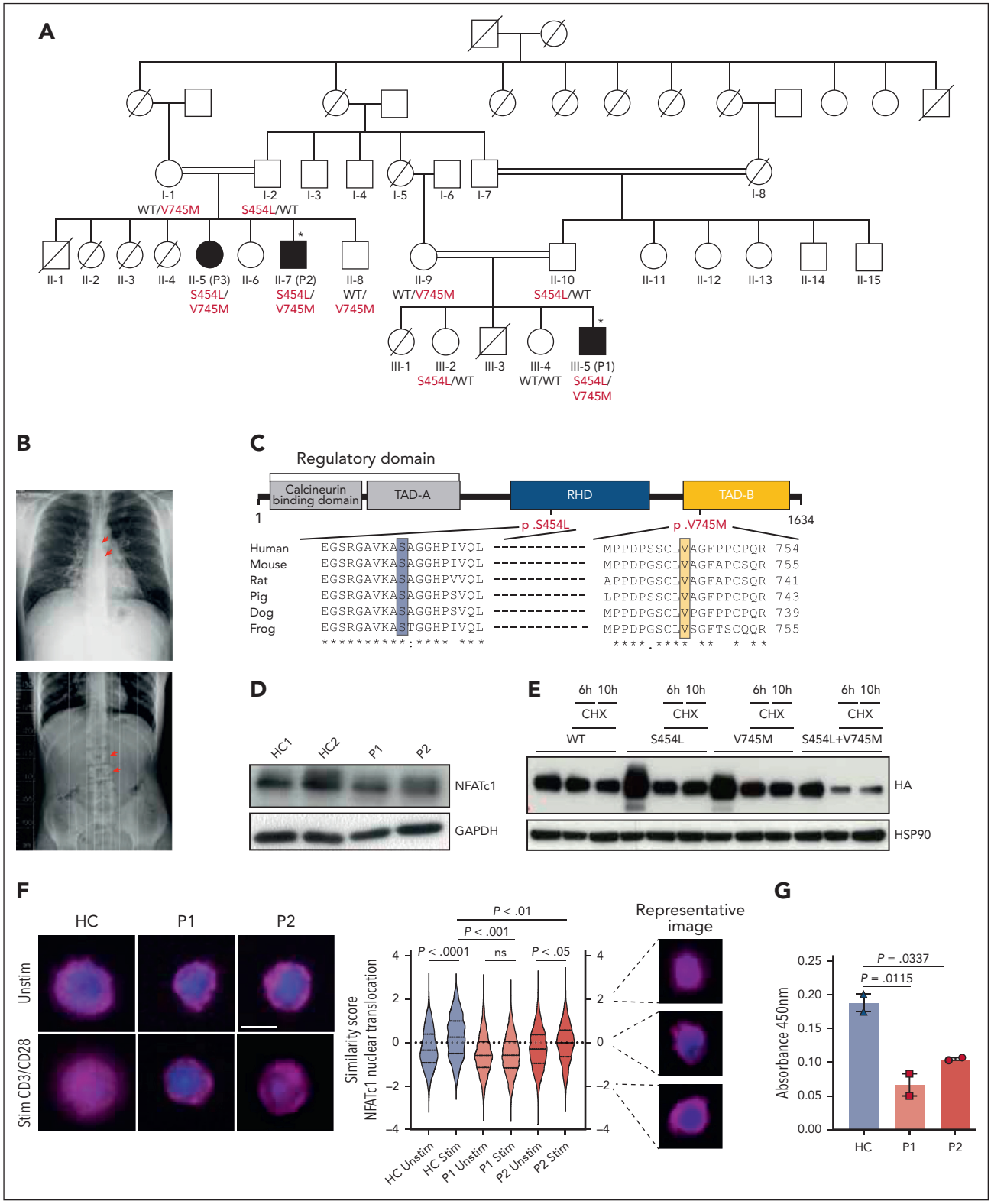

Figure 1. Identification of human *NFATC1* mutations and molecular analysis of the impact of identified variants on protein stability, localization, function, and interactions. (A) Pedigree of multigenerational family; shaded symbols, patients who are affected with compound heterozygous variants in *NFATC1*; open symbols, heterozygous carriers, individuals with wild-type genes or not genotyped. Double lines indicate consanguinity. Crossed symbols designate deceased individuals. The genotype of the patients and family members is indicated below each symbol. The asterisk represents those individuals who underwent WES. (B) Chest radiograph and thoracolumbal radiograph showing scoliosis in patients P1 and P2, respectively (red arrows). (C) Illustration of the NFATc1 protein, with N-terminal regulatory domain (Rel homology domain [RHD] and transactivation domain A [TAD-A]), for DNA binding to the consensus sequence, and C-terminal transactivation domain (TAD-B). Location of variants are shown together with their conservation across several species. An asterisk (*) indicates fully conserved; a colon (:), highly conserved; and a period (.), weakly conserved residues. (D) Immunoblot showing the NFATc1 expression in T cells from P1 and P2 (the patients whose material we could access) and HCs. (E) Representative blot for protein stability

CD3/CD28 stimulations were defective (supplemental Table 2). At present, P1 and P2 receive regular IV immunoglobulin (Ig) replacement and antibiotic prophylaxis, alleviating their symptoms. Detailed case reports are provided in the supplemental Information.

To unveil the genetic etiology, WES was performed on P1 and P2. Based on the pedigree, we assumed that there was an autosomal recessive mode of inheritance and extracted the data of all rare nonsynonymous homozygous and compound heterozygous variants shared between the affected relatives. Further analysis of compound heterozygous variants shared between the patients showed 2 missense variants within the *NFATC1* gene (ENST00000427363.7:c.1361C>T, p.S454L and ENST00000427363.7:c.2233G>A, p.V745M), further segregating the family members (supplemental Figure 2A). The variant p.S454L lies in the region Rel homology domain, critical for DNA binding in the groove proximal to the AP-1 binding site, and p.V745M is located in the transactivation domain B on the C-terminal end of the protein (Figure 1C). No homozygous cases of these variants were reported in the gnomAD database, and the frequency of observed heterozygous alleles were $<10^{-5}$ (last accessed, 14 April 2023). Notably both amino acids at their particular position were conserved across species (Figure 1C). Although the variants in additional genes were also segregated within the individuals, they were disregarded as being causative because they could not be related to the immunodeficiency status of the patients (supplemental Table 3). Collectively, these data suggested that the compound heterozygous constellation in *NFATC1* was potentially disease-causing.

Identified *NFATC1* variants result in reduced protein stability, DNA binding, nuclear translocation, and altered interaction with c-Jun

To elucidate the variants' pathogenic mechanisms, we tested their effect on the expression, localization, and function of NFATc1. Firstly, we measured the messenger RNA abundance and NFATc1 protein expression. Although messenger RNA levels were slightly higher, protein levels were comparable between patients (P1 and P2, the patients whose material we had access to) and HCs (Figure 1D; supplemental Figure 2B-C). Next, we assessed protein stability and found that ectopic expression of NFATc1^{S454L} and NFATc1^{V745M} variants exhibited reduced protein stability compared with wild-type NFATc1 (NFATc1^{WT}) in HEK-293T (human embryonic kidney) cells (Figure 1E; supplemental Figure 2D-E). Furthermore, we observed reduced NFATc1 nuclear translocation in stimulated T lymphoblasts from patient P1 compared with that in T lymphoblasts from the HC (Figure 1F; supplemental Figure 3). Furthermore, we detected a significant reduction in NFATc1 activation, as per enzyme-linked immunosorbent assay–based DNA binding, in patient T cells compared with that in HC cells (Figure 1G). Given that TFs operate by interacting with multiple proteins on promoter sites of target genes, we studied the impact of the NFATc1 variant proteins on their interaction with the AP-1 complex. Coimmunoprecipitation experiments demonstrated reduced interaction of both variants (more prominently in S454L) with c-Jun (supplemental Figure 4A). Taken together, our data indicate that both *NFATC1* variants affect protein function through decreased stability, cellular mislocalization, reduced activation, and aberrant interaction with c-Jun.

Dysfunctional NFATc1 impairs the differentiation, function, and survival of T cells

To systematically examine the effect of NFATc1 on lymphocyte differentiation, we performed detailed flow cytometric analysis on patient PBMCs. The overall proportions of T, B, and natural killer cells remained unaltered throughout the disease course (supplemental Table 2; supplemental Figure 4B-C). Within the T-cell population, CD8$^+$ T cells were increased, resulting in a decreased CD4:CD8 ratio in all 3 patients (supplemental Table 2). Despite the absence of autoimmunity, we detected lower proportions of Tregs and TfHs in patients (Figure 2A), consistent with that in NFATc1-deficient murine models, which have aberrant Treg and TfH development and disproportional Th1, Th2, and Th17 populations.[12] Interferon-γ (IFN-γ) and interleukin-4 (IL-4) productions were lower in CD4$^+$CD45 receptor α (RA)-negative T cells in patients, whereas the IL-17 production was comparable with that in HCs (supplemental Figure 4D). Similarly, CXCR3$^+$CCR6$^-$ populations as well as the GATA3 and T-Bet expression in Th2- (CCR4$^+$CCR6$^-$ CXCR3$^-$) and Th1- (CCR4$^-$CCR6$^-$ CXCR3$^+$) enriched populations were lower in patients than in HCs (supplemental Figure 4E-F). Both CD4$^+$ and CD8$^+$ T-cell compartments contained lower levels of naïve (CD45RA$^+$) and central memory T cells (CD45RA$^-$CCR7$^+$), with a corresponding increase in the effector memory T-cell (TEM:CD45RA$^-$CCR7$^-$) proportions (Figure 2B). Moreover, CD8$^+$ T cells displayed reduced CD28 but enhanced CD57 expression, attesting to their chronic activation and exhausted phenotype (Figure 2C; supplemental Figure 5). In summary, these results showed that patients harboring *NFATC1* mutations exhibited altered proportions of T-helper lineage, evidenced by reduced TfHs, Tregs, Th1s, and Th2s as well as aberrations in cytotoxic T cells.

NFATc1 plays a prominent role in T-cell effector functions, including cytokine (IL-2, IFN-γ, and tumor necrosis factor α) productions and cytotoxicity.[9,10,13] We therefore hypothesized

Figure 1 (continued) analysis using cycloheximide (CHX) chase assay on HEK cells transfected with either empty vector or Strep-HA-NFATc1^{WT}, -NFATc1^{S454L}, -NFATc1^{V745M}, or -NFATc1$^{V745M+S454L}$ plasmids, followed by 6 and 10 hours of CHX treatment. Quantifications of NFATc1 expression from blots represented in panels D and E are provided in Supplemental Figure 2B and D, respectively. (F) Representative images acquired with Image Flow Cytometer (AMNIS) (left), and similarity score quantification using IDEAS software (right) of NFATc1 nuclear translocation in feeder-expanded T lymphoblasts from patients or HCs, either without stimulation (Unstim) or upon stimulation with soluble anti-CD3/CD28 antibodies (Stim). Data show significant nuclear translocation in HC cells upon stimulation and no or slight nuclear translocation in T cells from patients P1 and P2, respectively. Representative images for different similarity scores (measure of nuclear translocation) in HCs are shown adjacent to the violin plot. Cells were stained with the nuclear marker DAPI (4′,6-diamidino-2-phenylindole) (blue); NFATc1 phycoerythrin is displayed in magenta. (G) Quantification of NFATc1 activation measured as absorbance at 450 nm using an enzyme-linked immunosorbent assay–based TF activation assay on feeder-expanded T lymphoblasts from patients or HCs after stimulation with phorbol 12-myristate 13-acetate (PMA) and ionomycin. All experiments are representative of at least 3 independent experiments with similar findings, with the exception of unstimulated fraction shown in panel G in which n = 1. All data are mean ± standard error of the mean (SEM) and were analyzed using 2-way analysis of variance (ANOVA) with Bonferroni post hoc test in panel F and one-way ANOVA with Bonferroni post hoc test to correct for multiple comparison in panel G. Scale bar, 5 μm; original magnification ×60 for panel F.

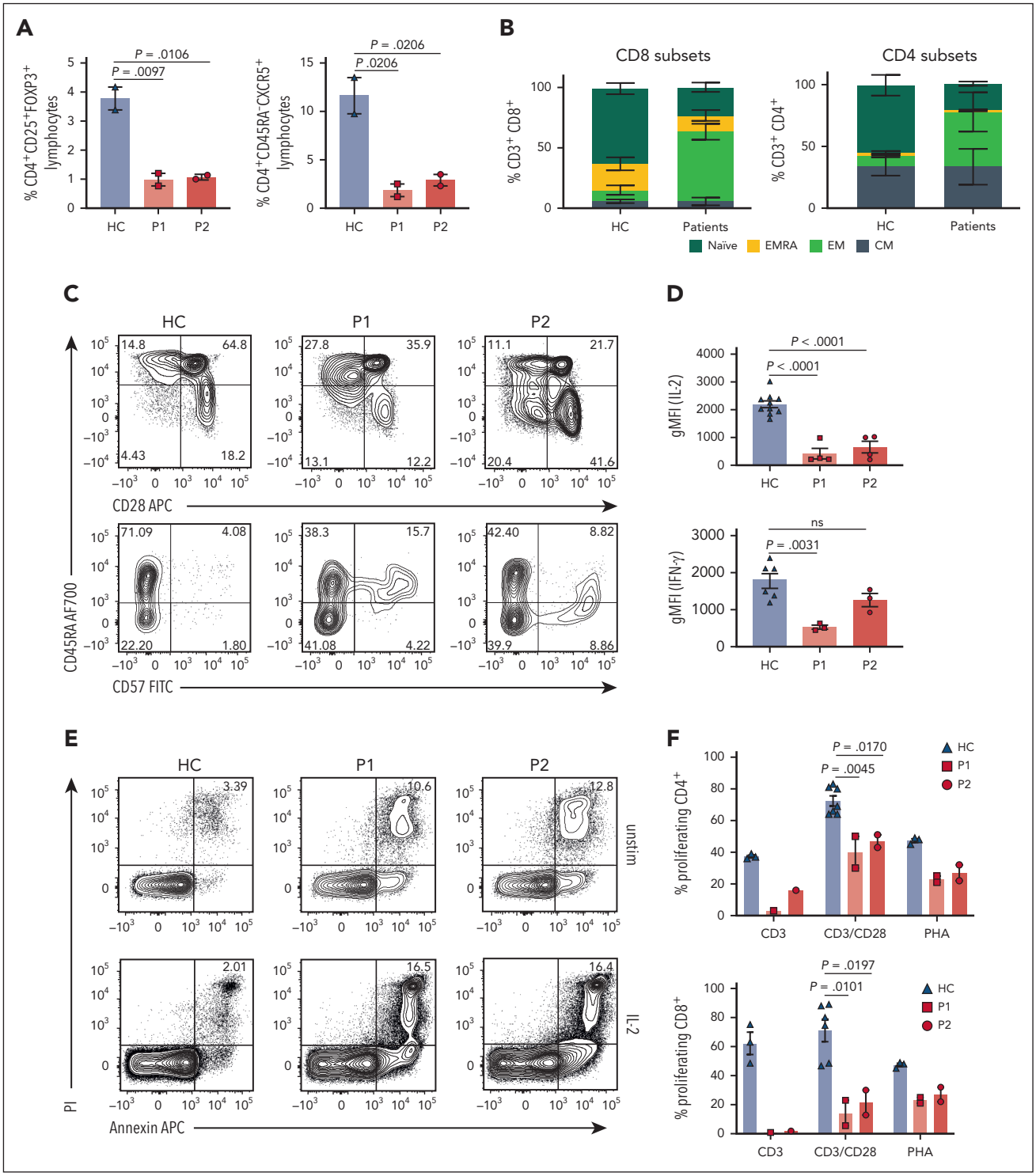

Figure 2. Dysfunctional NFATc1 impairs differentiation, effector function, and survival of T cells. (A) Proportions of Tregs (left) (Treg: $CD3^+CD4^+CD25^+FOXP3^+$) and TfHs (right) (TfH: $CD3^+CD4^+CD45RA^-CXCR5^+$), in HCs (n = 6) and patients (P1 and P2). (B) Proportions of naïve ($CD45RA^+CCR7^+$), central memory T-cell ($CD45RA^-CCR7^+$), T_{EM} ($CD45RA^-CCR7^-$) or T_{EMRA} (T–effector memory receptor alpha) ($CD45RA^+CCR7^-$) subpopulations within $CD4^+$ and $CD8^+$ fractions. (C) Flow cytometry dot plots quantitating surface CD28 and CD57 expression on $CD8^+$ T cells. (D) Summary bar graphs showing quantification of IL-2 (upper panel) or IFN-γ (lower panel) intracellular expression determined via flow cytometric analysis. T lymphoblasts were analyzed for IL-2 and IFN-γ production after 5 hours of PMA/ionomycin stimulation and addition of brefeldin A during the final 4 hours. Surface staining was performed with CD3, CD4, CD8, and $CD3^+CD8^+$ cells were gated. (E) Flow cytometry plots showing the percentage of apoptotic cells in feeder-expanded T lymphoblasts, measured via annexin-V and propidium iodide staining, after withdrawing IL-2 from the growth media (top plot) and after 24 hours treatment with IL-2 (200 IU/μL) (bottom plot). (F) Summary bar graphs showing the percentage of proliferating cells as measured by the dilution of the violet proliferation dye (VPD450) in $CD4^+$ and $CD8^+$ T cells from the patients and HCs after 3 days of stimulation with anti-CD3 soluble antibody, CD3/CD28 beads, or phytohemagglutinin (PHA). (G) Summary bar graphs showing percentage of $CD4^+$ and $CD8^+$ T cells that have upregulated CD25 surface expression at day 3, corresponding to the proliferation experiments shown in panel F. (H) Representative histogram showing the dilution of VPD450 in the green fluorescent protein–positive (GFP^+) population of the patient $CD8^+$ T cells transfected with either the GFP-$NFATc1^{WT}$ (red) or GFP-empty (blue) plasmids at day 3, upon stimulation with CD3/CD28 beads. Summary plots of the percentage

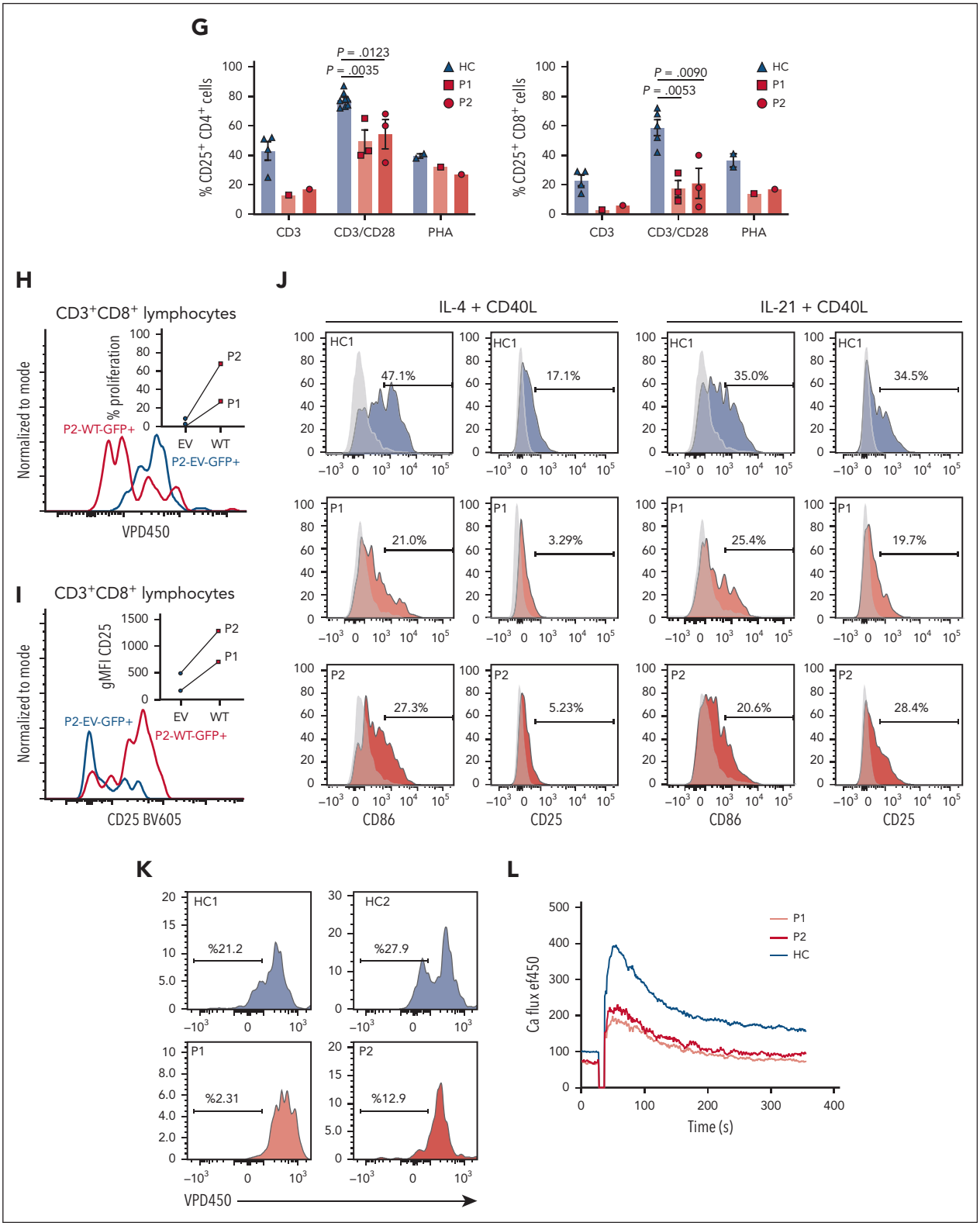

Figure 2 (continued) of proliferating cells after transfection of both patients' PBMCs are shown in the upper square within the graph. (I) Representative histogram showing CD25 expression normalized to mode of GFP$^+$ CD8$^+$ T cells on day 3, corresponding to the experiments shown in panel H. Summary plots of CD25 expression, after transfection of both patients' PBMCs are shown in the upper square within the graph. (J) Flow cytometry histograms quantitating surface CD86 and CD25 expression on CD19 cells of patients and HCs after 48 hours stimulation with CD40L and IL-4 or CD40L and IL-21. (K) Representative histogram showing the dilution of VPD450 in CD19 B cells from patients and HCs after 5 days of stimulation with CpG. (L) Representative flow cytometry plot showing Ca^{2+} influx in EBV-transformed B lymphoblasts from patients P1 and P2 and HCs upon 100 nM ionomycin treatment as measured by Ca^{2+}eFluor450 dye expression. All data are mean ± SEM. Statistical analysis in panels A, D, F, and G was performed using a one-way ANOVA with Bonferroni post hoc test to correct for multiple comparison. EV, empty vector; gMFI, geometric mean fluorescent intensity.

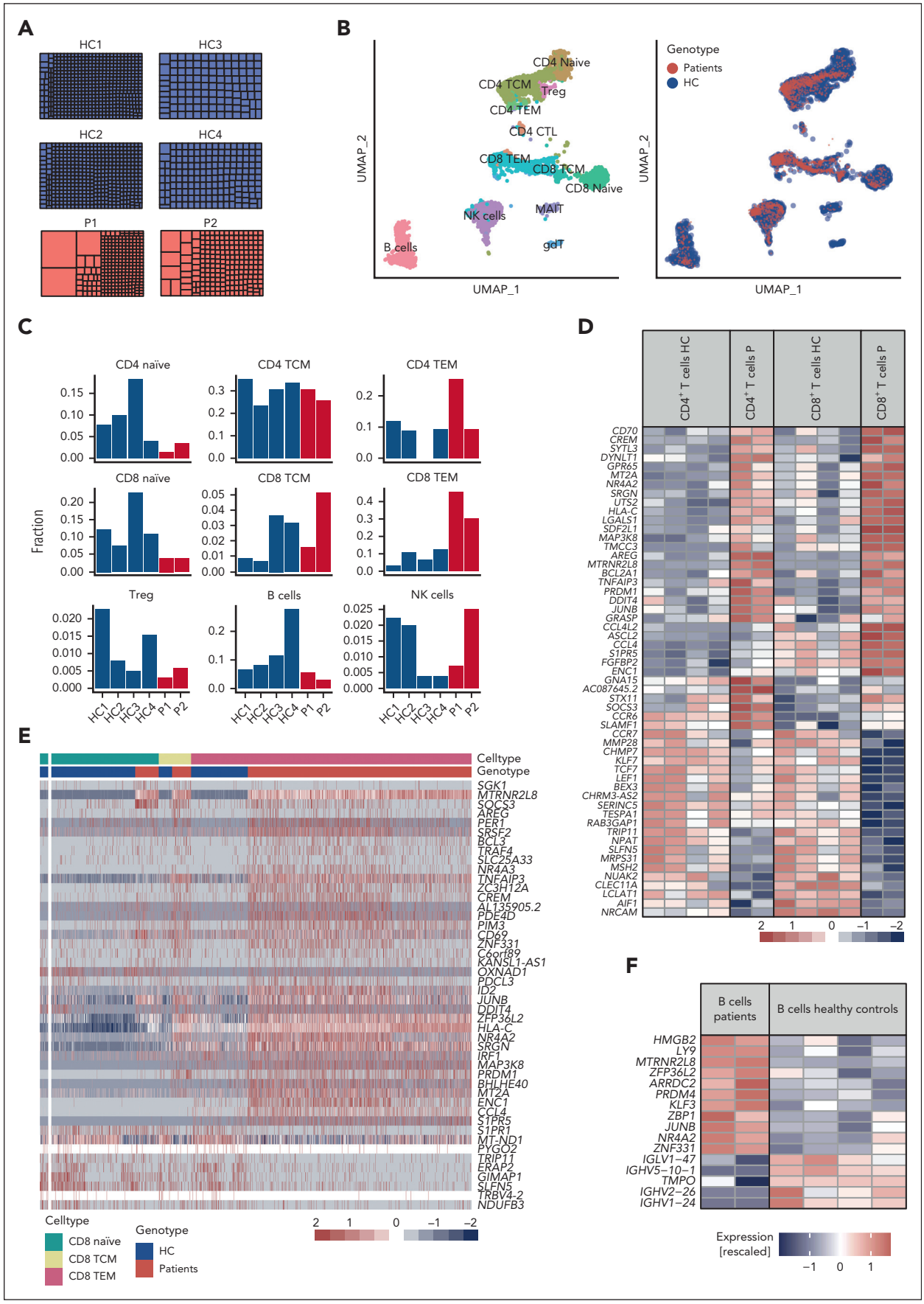

Figure 3.

that *NFATC1* LOF would compromise the effector responses of T cells. Indeed, upon stimulation, patient T lymphoblasts exhibited diminished IL-2 and IFN-γ production (Figure 2D) as well as reduced expression of CD107a, indicating compromised lytic machinery (supplemental Figure 6A). NFAT transcriptional control is essential for maintaining survival,[5,13-15] and, indeed, patient $CD8^+$ T lymphoblasts showed higher apoptosis compared with those of HCs, which could not be rescued by IL-2 (Figure 2E). To exclude the possibility of an additional signaling defect that would impair T-cell functions, we tested the signaling cascades and Ca^{2+} flux after TCR stimulation. Except for a slight reduction of protein kinase B (AKT) phosphorylation, the downstream TCR responses (Ca^{2+} flux and extracellular signal-regulated kinase, p65, and S6 phosphorylation) remained intact (supplemental Figure 6B-C), ruling out additional defects proximal to NFAT signaling that might contribute to cellular dysfunctions. Consistent with the role of Nfatc1 in T-cell activation and proliferation in murine models,[16,17] patient PBMCs showed defective proliferation and CD25 upregulation compared with that of the PBMCs from HCs, predominantly in the $CD8^+$ T-cell population (Figure 2F-G) and even more pronounced in the naïve T-cell compartment (supplemental Figure 6D). Importantly, genetic reconstitution of WT *NFATC1* into patient PBMCs restored both stimulation-induced CD25 expression and proliferation (Figure 2H-I), proving the pathogenicity of the patients' inherited *NFATC1* variants.

NFATc1 is required for survival and proliferation of activated mature B-cell populations

The Ca^{2+}/NFAT axis is critical for germinal center reactions, implicated in the regulation of inducible costimulator and CD40L expression and, thus, TfH differentiation.[12] After TCR stimulation, there was reduced upregulation of CD40L in patient TfHs compared with HCs (supplemental Figure 6E). Despite normal absolute $CD19^+$ B-cell numbers, we detected a phenotypic skewing of B-cell subsets with slightly lower switched-memory proportions and increased naïve B cells in patients (supplemental Figure 4C). These data are reminiscent of the mild effect on B-cell differentiation processes in the bone marrow and periphery of NFATc1-deficient murine models.[18] However, these mice have blunt cell proliferation and Ca^{2+} flux responses to stimulation, culminating in decreased Ig class switch and plasmablast formation as well as aberrant cellular immune responses.[18] Therefore, we subsequently assessed functional responses in patient B cells. Compared with $CD19^+$ B cells from HCs, patient cells were less responsive to stimulation with CD40L and IL-4, as assessed via CD86 upregulation (Figure 2J). Notably, the activation marker CD25 was only partially upregulated in patient B cells, suggesting impaired IL-2–mediated survival and proliferation (Figure 2J). In response to CD40L and IL-4/IL-21 as well as cytosine–phosphate–guanosine (CpG) stimulations, patient B cells were capable of class switch recombination to IgG in vitro, albeit with reduced frequency at day 7 (supplemental Figure 7A), an effect likely due to impaired proliferative capacity, which was lower after CpG exposure (Figure 2K). Given the reported Ca^{2+} flux perturbations in peripheral B cells from NFATc1-deficient mice,[18] we tested Ca^{2+} dynamics in patient Epstein-Barr virus (EBV) B cells. Patient-derived EBV B cells displayed reduced Ca^{2+} flux upon ionomycin treatment (Figure 2L), an effect that was rescued upon transfection with WT-*NFATC1* vector on P1 EBV B cells (supplemental Figure 7B). These data added corroborating evidence regarding the causality of the dysfunctional NFATc1 leading to an impaired B-cell function in patients. Taken together, these results suggest that intact NFATc1 is required to relay signals essential for survival and proliferation of activated mature B-cell populations.

Transcriptomic analysis of NFATc1 patient lymphocytes indicates chronic inflammation and a tolerogenic/senescent signature

To better understand how NFATc1 dysfunction affects patient lymphocytes, we compared the basal transcriptome and TCR repertoire of lymphocytes between P1 and P2 and HCs using droplet-based single-cell RNA sequencing (10x Genomics). The number of TCRαβ clonotypes in patient T-cell populations, particularly within the $CD8^+$ TEM fraction (supplemental Figure 8), were lower than that in HC T cells, indicating a diminished TCRαβ repertoire diversity (Figure 3A). Consistent with our flow cytometric immunophenotyping (Figure 2B), transcriptional profiling confirmed reduced naïve $CD4^+$ and $CD8^+$ T cells, with a concomitant skewing toward a TEM phenotype (Figure 3B-C), as well as reduced Tregs and decreased CCR7 and IL-7RA expression, similar to the observations in NFATc1-deficient murine models.[10]

Differential gene expression analysis of $CD4^+$ and $CD8^+$ T cells from patients (Figure 3D) showed increased transcription of genes associated with chronic inflammation (*CD70, GPR65, JUNB,* and *MAP3K8*),[20] cellular stress (*MTRNRL2* and *SDF2L1*),[21-23] and tolerogenic signals (*LGALS1, CREM, AREG,* and *NR4A2*) compared with HCs.[24-26] Consistently, an activated and terminally differentiated effector state (*PRDM1*)[27] was further evidenced by reduced *TCF7*, *LEF1*, and *KLF7* expressions in the $CD8^+$ compartment,[25,28,29] altogether corroborating the molecular evidence for an anergic/exhausted state of patient T cells (Figure 3D). We performed a gene set enrichment analysis on 16 predefined pathways (supplemental Table 8) and detected a significant enrichment in anergy/exhaustion pathways in patients compared with those in HCs

Figure 3. Single-cell RNA sequencing reveals the altered transcriptomic profile of patients with dysfunctional NFATc1. Basal transcriptome and profiled TCR repertoire of lymphocytes from P1 and P2 compared with that of HCs via single-cell RNA sequencing (5′ scRNAseq, 10x Genomics). (A) Analysis of TCR antibody repertoire diversity with a tree-map representation for patients P1 and P2 and age-matched HCs. Each square represents a unique clone and its size reflects its productive frequency within the repertoire. (B) Uniform manifold approximation and projection plot of the combined scRNAseq data set from P1, P2, and HCs. (Left) Cells colored based on cell type annotation after mapping to a reference data set of healthy PBMC,[19] cell types with <20 cells omitted for clarity. (Right) Cells colored based on the genotype; patient data shown above HC data. (C) Bar graphs showing proportions of different cell populations within the lymphocytes. (D) Heatmap showing pseudobulk expression data for genes (shown as rows) that are differentially expressed between patients and HCs within $CD4^+$ and $CD8^+$ T-cell populations (samples and cell types shown as columns). Genes shown are the top 20 up- or downregulated in any of the 2 tests (tests performed with edgeR software with exact test and pseudobulk data; false discovery rate < 0.05; ranked based on the *P* value). Expression values shown are scaled log counts per million cropped to the range −2 to 2. (E) Heatmap showing single-cell expression data for genes differentially expressed between patients and HCs within $CD8^+$ T-cell subpopulations (naïve, TCM [central memory T cells] and TEM [effector memory T cells]). Genes shown are the top 30 up- or downregulated in any of the 2 tests (tests performed as in panel D). (F) Heatmap showing single-cell pseudobulk expression data for genes differentially expressed between patients and HCs within $CD19^+$ B cells (tests performed as in panel D).

(hypergeometric test, false discovery rate ≤ 0.05).[30] We assessed the altered expression of selected marker genes at protein level (CD70 and PRDM1) via flow cytometry (supplemental Figure 9). We then focused on the expression profile within the CD8$^+$ TEM compartment, constituting the largest CD8$^+$ T-cell fraction having a differential distribution among the HCs and patients. Interestingly, within this population, we observed a significant increase in genes including *SGK1* and *PIM3*, implicated in connecting T-cell–fate determination to cellular metabolic signals such as environmental nutrient deprivation and/or mammalian target of rapamycin (mTOR) activation[31,32] (Figure 3E). Collectively, transcriptome

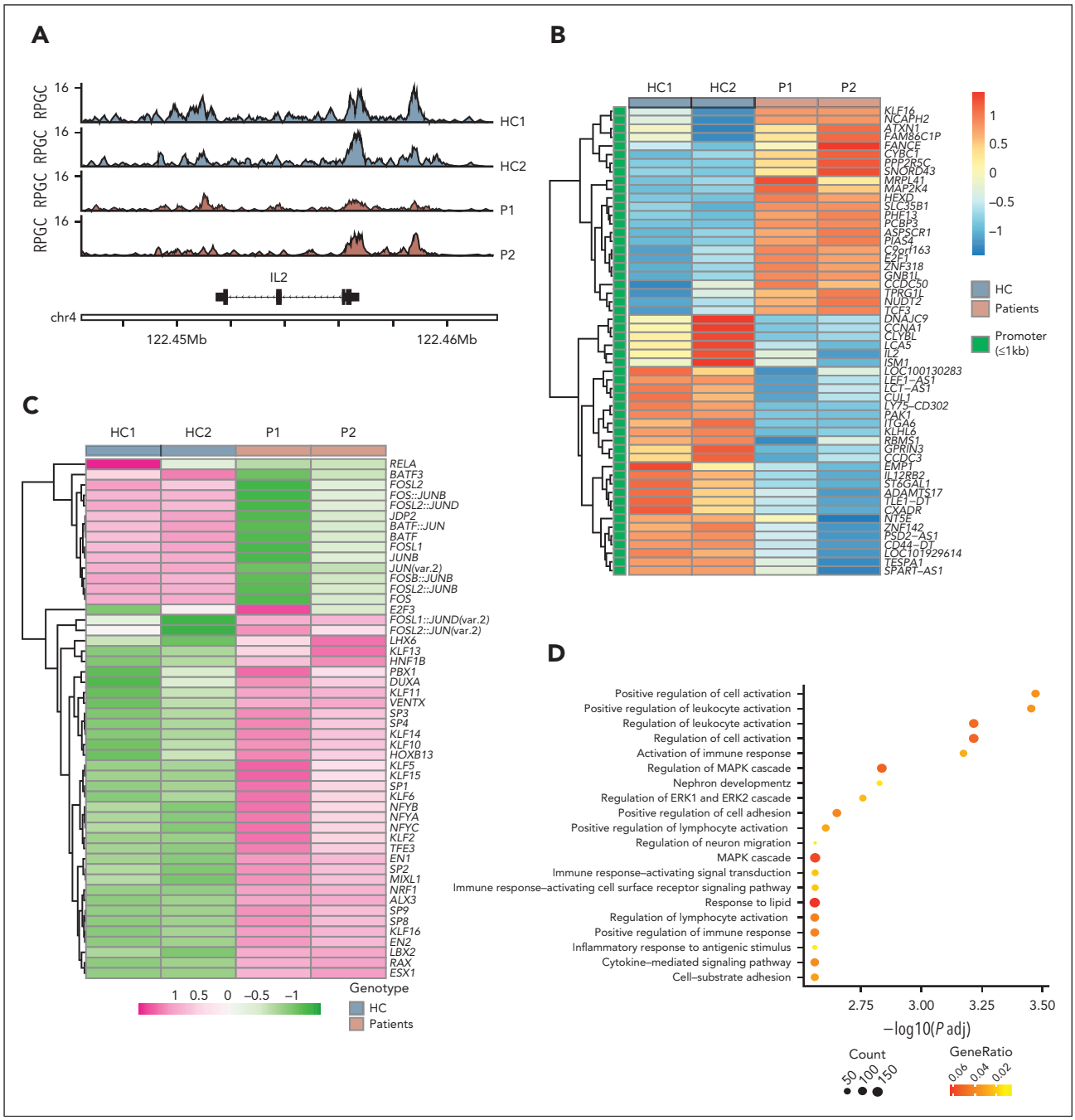

Figure 4. Altered epigenome landscape of patient T lymphoblasts. We performed an ATACseq using patient and HC T lymphoblasts upon stimulation with PMA/ionomycin to initiate downstream epigenetic and transcriptional changes. (A) ATACseq chromatogram showing the accessibility of *IL2* gene locus in patients P1 and P2 and HCs (n = 2). Reads per genomic content (RPGC; 1 × normalization) normalized tracks. (B) Heatmap of differentially accessible regions at gene promoters (transcription start site ± 1 kb) between HC-derived (HC1 and HC2) and patient-derived (P1 and P2) expanded T cells [DESeq2; abs(log2FC) > log2(1.3)].[35] Values are *z* scores derived from regularized log transformation (DESeq2 rlog function) of count data. Positive values indicate that regions of the corresponding genes are more transcriptionally accessible, whereas negative values indicate that the regions are less accessible. (C) Heatmap of top 50 most significantly (P_{adj} < .05; a Benjamini-Hochberg [BH] adjusted *P* value for the variability being greater than the null hypothesis of 1) variable transcription factor motifs across samples of HC-derived (HC1 and HC2) and patient-derived (P1 and P2) expanded T cells. Values are z scores for each bias-corrected deviations. (D) Top 20 significantly (P_{adj} < .05); a BH adjusted corrected *P* value (*P* < .05) and HC-only enriched GOBP (gene ontology biological processes) terms of genes associated with unique WT peaks.

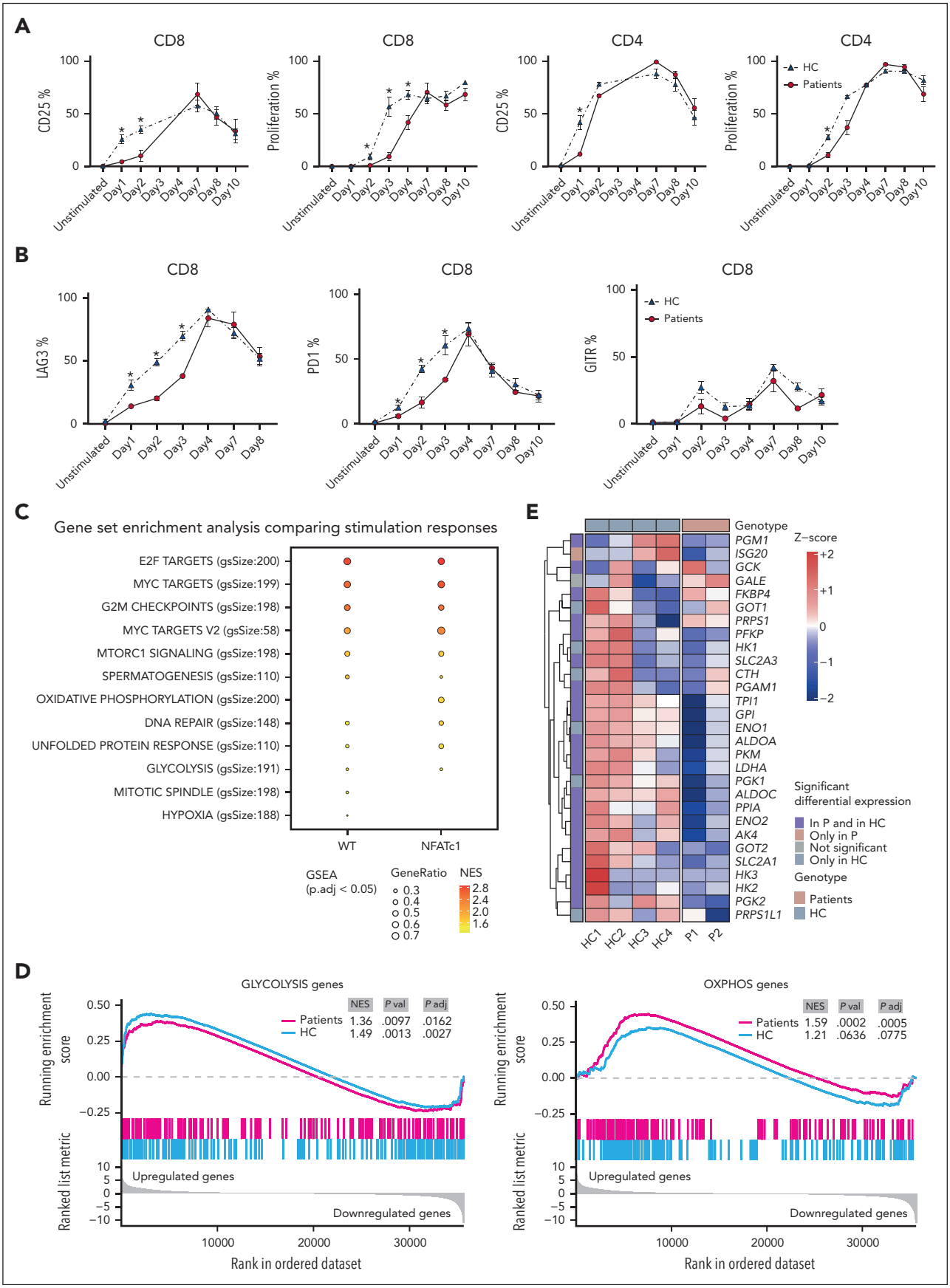

Figure 5.

profiling of patients with dysfunctional NFATc1 revealed a state of chronic activation and increased cellular stress response and anergy in T cells.

Within the B-cell compartment, differential gene expression analysis revealed 16 genes that had altered expression levels in the patients compared with those in HCs. Interestingly, we detected reduced expression of several Ig heavy and light chain genes, including *IGHV5-10-1*, *IGHV1-24*, *IGHV1-26*, and *IGLV1-47* (Figure 3F), similar to the NFATc1-deficient murine models, suggesting a role for NFATc1 as a facilitator of Ig gene locus accessibility.[33] Pathway analysis of upregulated genes confirmed a proinflammatory state in patients, with a significant enrichment in tumor necrosis factor α/NF-κB signaling (supplemental Table 9). Upregulation of genes such as *ZFP36L2*, *KLF3*, *PRDM4*, and *ZBP1*, which are usually expected to be downregulated during the transition from naïve to mature B cells, suggested a differentiation defect. Consistently, we detected a reduced differentiation to plasmablasts ($CD19^+CD27^+CD38^+$) upon stimulation with CD40L and IL-4 or IL-21 (supplemental Figure 10).

Altered global chromatin landscape in human NFATc1 dysfunction

NFATc1 regulates chromatin remodeling and increases DNA accessibility to interacting TFs.[34] Based on our earlier data showing reduced binding of NFATc1 to DNA and AP-1 complex, we hypothesized reduced accessibility of NFAT mutants at the NFAT sites of the *IL2* promoter. Thus, we performed an assay for transposase-accessible chromatin with high-throughput sequencing (ATACseq) on stimulated T lymphoblasts of patients and HCs. Analysis of the consensus peaks at the promoter sites confirmed a decreased accessibility of the *IL2* promoter (Figure 4A), alongside other genes involved in T-cell proliferation and effector responses (*CCNA1*, *TESPA1*, *IL12RB2*, *CD44*, *PAK1*, and *LEF1*) in patients compared with that in HCs (Figure 4B). The motif heatmap (Figure 4C) shows z scores of chromatin accessibility for the top 50 most significantly ($P_{adj} < .05$) variable motifs across samples. The majority of the FOS-JUN motifs, as well as several other AP-1 complex family members, including basic leucine zipper transcriptional factor ATF-like (BATF), have a reduced pattern of chromatin accessibility in patients compared with that in HCs. AP-1 transcription complex comprises numerous basic region leucine zipper proteins that belong to different families (JUN, FOS, ATF, BATF, and MAF) and form heterodimers to execute transcriptional activity. The members of this family, such as BATF, might control genes other than the typical c-JUN/cFOS heterodimers or can replace such heterodimers under different physiological conditions.[36,37] Collectively, ATACseq data suggest an overall reduced chromatin accessibility for AP-1 complex motifs in patient cells. Gene ontology term enrichment analysis of unique accessibility sites for patients and HCs revealed HC-specific gene ontology enrichments of the genes involved in adaptive immune response, effector functions, and activation responses, implying reduced accessibility of corresponding sites in patient cells (Figure 4D). Altogether, these data support our earlier findings on reduced IL-2 production caused by dysfunctional NFATc1 in patient T cells, with reduced accessibility of the chromatin regions required for T-cell activation.

NFATc1 dysfunction delays T-cell activation, which is associated with perturbed metabolic responses

To better understand the effect of NFATc1 deficiency on the temporal patterning of T-cell activation and proliferation responses, we performed detailed time-course experiments. Interestingly, determinants of activation and proliferation, which were clearly different at earlier time points, were no longer distinguishable between $CD8^+$ T cells of patients and those of HCs 7 days after stimulation (Figure 5A). Because NFATc1 fine-tunes the activation and senescence processes,[8] we assessed the expression profile of checkpoint inhibitors typically upregulated upon TCR activation in parallel to surface CD25. We observed a delayed upregulation of PD-1, LAG3, and AITR/GITR upon TCR stimulation, particularly in patient $CD8^+$ T cells in a trend reminiscent of the delayed activation (Figure 5B; supplemental Figure 11A). A slight reduction in activation and proliferation was evident in $CD4^+$ cells, albeit to a lesser extent than that in the $CD8^+$ T cells, whereas exhaustion parameters were comparable (supplemental Figure 11B). We hypothesized that the delay in activation is preceded by an altered transcriptional program in patient T cells. Thus, we stimulated PBMCs until day 3, which corresponded to the time point at which the largest difference in proliferation between patient and HC cells was observed, and performed bulk RNA sequencing on sorted $CD8^+$ T cells. We analyzed enrichment of gene sets for 50 hallmark functions and pathways[38] by calculating the normalized enrichment score (NES), which represents enrichment of genes from a tested gene set toward the top of the ranked list (positive NES) or the bottom of the ranked list (negative NES). Our data set shows the gene enrichment profile of the stimulated T cells in comparison with that of unstimulated cells. TCR stimulation induced a global increase in the signals from pathways regulating the cell cycle, ribosomal organization, protein translation, and unfolded protein response as well as metabolic signatures, including mTOR signaling in both HCs and patients (Figure 5C-D). In patients, a statistically significant positive enrichment is present for OXPHOS in the upregulated

Figure 5. Time-course analysis of proliferation, activation, and upregulation of checkpoint inhibitors of T cells in parallel to RNA sequencing reveals their delayed responses associated with perturbed metabolism. (A) Representative graphs showing the percentage of $CD4^+$ or $CD8^+$ T cells with upregulated CD25 surface expression after stimulation with CD3/CD28 beads and percentage of proliferation by measuring the dilution of VPD450 in $CD4^+$ and $CD8^+$ T cells from patients and 3 HCs at basal state (unstimulated), and on days 1, 2, 3, 4, 7, and 8 (and day 10 for PD1 and GITR) after stimulation. Marker up/downregulation was measured via flow cytometry at basal state (before stimulation), and on days 1, 2, 3, 4, 7, and 8 (and day 10 for PD1 and GITR) after stimulation. (B) Summary graphs showing the percentage of $CD8^+$ T cells that have upregulated PD1, LAG3, AITR/GITR surface expression after stimulation with CD3/CD28 beads measured via flow cytometry at basal state (unstimulated), and on days 1, 2, 3, 4, 7, and 8 (and day 10 for PD1 and GITR) after stimulation. (C) PBMCs from patients and 4 HCs were stimulated with CD3/CD28 beads, and on the third day after stimulation $CD8^+$ T cells were sorted via flow cytometry. Bulk RNA sequencing was performed on sorted $CD8^+$ T cells. Plots show the gene set enrichment analysis of 50 hallmark functions based on calculated NES. Pathways are stratified for the top 10 most significantly upregulated pathways upon stimulation comparing patients and the HCs. (D) Plots showing the calculation of ranking of NES within gene set enrichment analysis from hallmark databases representing the stimulation-induced changes in expression of $CD8^+$ T cells in patients and HCs with regard to OXPHOS (right) and glycolysis gene sets (left). (E) Heatmap showing the expression of genes involved in glucose metabolism extracted from bulk RNA-sequencing analysis. Significance for gene expressions is indicated in panel E.

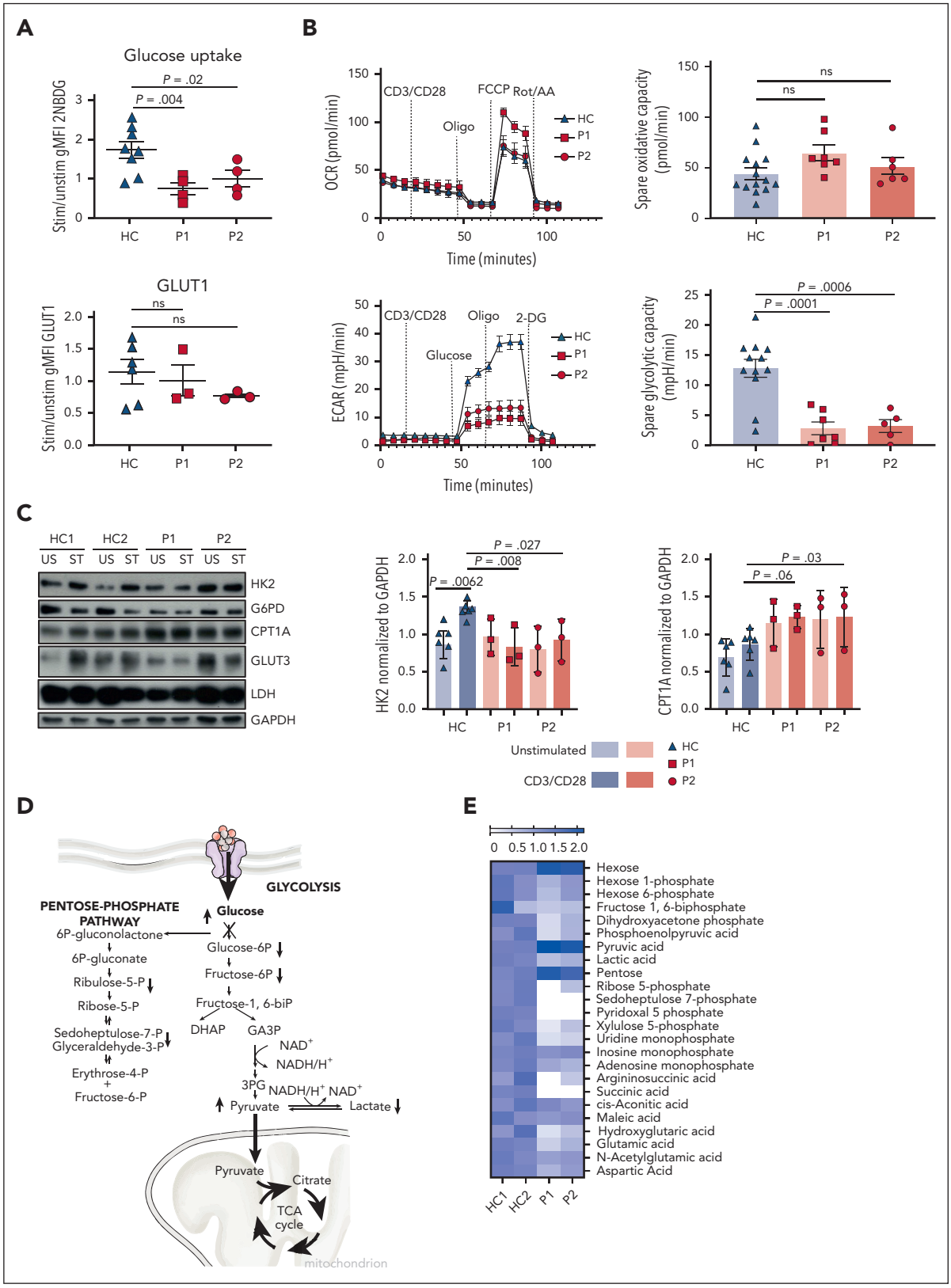

Figure 6. Metabolic profiling of NFATc1-dysfunctional T cells shows impaired glycolysis upon stimulation. (A) Summary dot plots showing the ratio of change of expression level of glucose transporter 1 (GLUT1) and glucose uptake using fluorescent glucose analog 2-NBDG after 24-hour stimulation of feeder-expanded T cells with soluble CD3/CD28 antibodies measured by gMFI. (B) Extracellular flux analysis. (Top) Graph showing oxidative consumption rate of HC (n = 3) and patient CD8$^+$ T lymphoblasts after 30 minutes stimulation with CD3/CD28 beads and subjected to mitochondrial stress test. (Bottom) Graph showing extracellular acidification rate of HC (n = 3) and patient CD8$^+$ T lymphoblasts, which were stimulated for 30 minutes with CD3/CD28 beads and subjected to glycolytic stress test. Experimental data were normalized to flow cytometric cell counts. (C, left) Immunoblot showing the protein expression levels of HK2, glucose transporter-3 (GLUT3), carnitine palmitoyl transferase 1a (CPT1a),

gene set upon stimulation compared with the unstimulated samples, whereas in HCs, the contribution of oxidative pathway genes to the upregulated data set was not significant. These data reveal a transcriptional disconnect between the expression profiles induced upon activation in HC compared with NFATc1-defective cells.

Given the impaired glycolysis in NFATc1-deficient murine models,[10] we then focused on the genes regulating glycolysis (such as *HK2*, *ENO*, *PGK2*, and *PFK2*) and observed a differentially reduced expression pattern in patients compared with that in HCs (Figure 5E). These data prompted us to analyze the metabolic parameters and functional capacity of patient T cells. We assessed glucose uptake in activated $CD8^+$ T lymphoblasts using the fluorescent glucose analog 2-NBDG (2-[N-(7-nitrobenz-2-oxa-1,3-diazol-4-yl)amino]-2-deoxy-D-glucose) and observed that patient cells took up less glucose than HC cells despite equivalent GLUT1 surface levels (Figure 6A; supplemental Figure 12A-B). Next, we detected a lower glycolytic rate and glycolytic reserve capacity in patient $CD8^+$ T lymphoblasts upon stimulation compared with that in HC. Conversely, no major effect was observed on OXPHOS and mitochondrial respiration in patient T lymphoblasts (Figure 6B). These findings, including reduced glucose uptake and glycolysis capacity due to an altered transcriptome, phenocopy those of $CD8^+$ T cells from *Nfatc1*$^{-/-}$ mice.[10] Consistent with hexokinase 2 (HK2; a glycolytic marker) expression being regulated by NFATc1,[10] we observed that the stimulation-induced increase in HK2 expression was almost absent in P1 and reduced in P2 T lymphoblasts, whereas the expression of GLUT3, a major glucose transporter in addition to GLUT1,[39] remained unaltered (Figure 6C-D; supplemental Figure 12-13). Accordingly, liquid chromatography mass spectrometry metabolomics analysis revealed higher hexose (representing glucose) and pentose levels with a concomitant decrease in downstream glycolytic metabolites in patient T cells, consistent with an obstructed initial step of glycolysis (Figure 6E).

NFATc1-mutant T cells compensate for impaired glycolysis by enhancing lipid metabolism

The observation that the delayed patient T-cell activation and proliferation responses could "catch up" prompted us to evaluate whether NFATc1-dysfunctional cells could adapt by increasing their reliance on alternative metabolic substrates. Not only was the expression of CPT1a, a transporter of FAs to the mitochondria and key regulator of FA metabolism, higher in stimulated patient T cells (Figure 6C-D; supplemental Figure 13), but lipid uptake determined using Bodipy FL C16 was also higher in patient T lymphoblasts, both with and without stimulation, compared with that in HCs (Figure 7A; supplemental Figure 14A). Interestingly, lipidomic analysis revealed that although overall lipid populations increased upon stimulation in both HC and patient cells (Figure 7B), consistent with the stimulation-induced increase in lipid uptake observed via Bodipy (Figure 7A). The extent of the increase in the triacylglycerol pool is markedly attenuated in patient cells compared with HC cells (Figure 7C-D). Together, these data suggest that patient cells had a shifted substrate preference toward FA oxidation (FAO). Indeed, fluxomic experiments using [$^{13}C_{16}$]-palmitic acid revealed patient T lymphoblasts to have higher tracer incorporation into citrate isotopologues, indicating enhanced flux of exogenously administered, palmitate-derived carbons into the tricarboxylic acid (TCA) cycle (Figure 7E). Considering the exhausted phenotype of the patient cells and heterogeneity in the T-cell pool, we sought innovative ways to delineate, at the T-cell subpopulation level, the consequences of the *NFATC1* mutations on metabolic responses. We used the recently described flow cytometry–based metabolic profiling technique SCENITH and extended our understanding at the single-cell level.[40] Although patient $CD4^+$ T cells displayed similar metabolic trends compared with those of HC cells (supplemental Figure 14B), consistent with the impaired glycolytic capacity observed in patient T lymphoblasts during the glycolysis stress test (Figure 6B), further analysis of the $CD8^+$ T-cell subpopulation revealed that the TEM ($CD45RA^-CCR7^+$) population was most different compared with that of HCs (Figure 7F) and, thus, most sensitive to NFATc1 deficiency. Taken together, these data strongly support the argument that *NFATC1* mutations impair glycolysis in $CD8^+$ T cells, which is associated with delayed CD8 T-cell effector responses and a metabolic shift toward β-oxidation and FA use.

Pharmacological modeling of patient phenotype in primary T cells recapitulates the metabolic flexibility observed in patient cells

To better understand the molecular association between the impaired glycolysis in the NFATc1-dysfunctional patient cells and the adaptation toward FAO, we aimed to pharmacologically model the patient phenotype using lymphocytes derived only from HCs. Consistent with established literature, inhibiting glycolysis in HC PBMCs using 2-deoxyglucose (2-DG) reduced activation and proliferation.[1,2] In contrast to NFATc1-deficient mice,[10] such defects in activation and proliferation, secondary to ablated glycolysis, could not be rescued with IL-2 treatment (supplemental Figure 14C-D). Next, we assessed the effect of 2-DG on IL-2 production of HC lymphoblasts. Lower IL-2 production upon 2-DG treatment further corroborated the necessity of glycolysis for appropriate effector responses (supplemental Figure 14E). To rule out the possibility that the defects in activation and proliferation responses in patient PBMCs merely reflected differences in T-cell subset proportions, we performed time-course experiments in sorted HC naïve T cells treated with cyclosporin A (CsA)[41] to model NFAT inhibition or with 2-DG to inhibit glycolysis and measured their functional and metabolic responses. In a pattern reminiscent of that observed in patient cells, stimulated $CD8^+$ T cells exposed

Figure 6 (continued) glyceraldehyde 3-phosphate dehydrogenase (GAPDH), and lactate dehydrogenase (LDH) on patient and HC T lymphoblasts with (ST) and without (US) 24-hour stimulation using soluble anti-CD3/CD28 antibodies. (C, right) Graphs showing the quantification of the western blots averaged from 3 independent experiments displaying the expressions of HK2 and CPT1a. (D) Scheme summarizing the metabolic alteration observed in patient T lymphoblasts after stimulation. (E) Heatmap showing fold changes of metabolite concentrations (stimulated/unstimulated) in T lymphoblasts in patients and HCs measured by metabolomics after 24 hours of stimulation with soluble anti-CD3/CD28 antibodies. All data are mean ± SEM. Statistical analysis was performed using one-way ANOVA with Bonferroni post hoc test (A-B) or 2-way ANOVA with Bonferroni post hoc test (C) to correct for multiple comparison. AA, antimycin A; DHAP, dihydroxyacetonephosphate; FCCP, carbonyl cyanide-p-trifluoromethoxyphenylhydrazone; GA3P, glyceraldehyde 3-phosphate; NAD, nicotinamide adenine dinucleotide; NAD(H), nicotinamide adenine dinucleotide+hydrogen; oligo, oligomycin; 3-PG, 3-phosphoglycerate; Rot, rotenone.

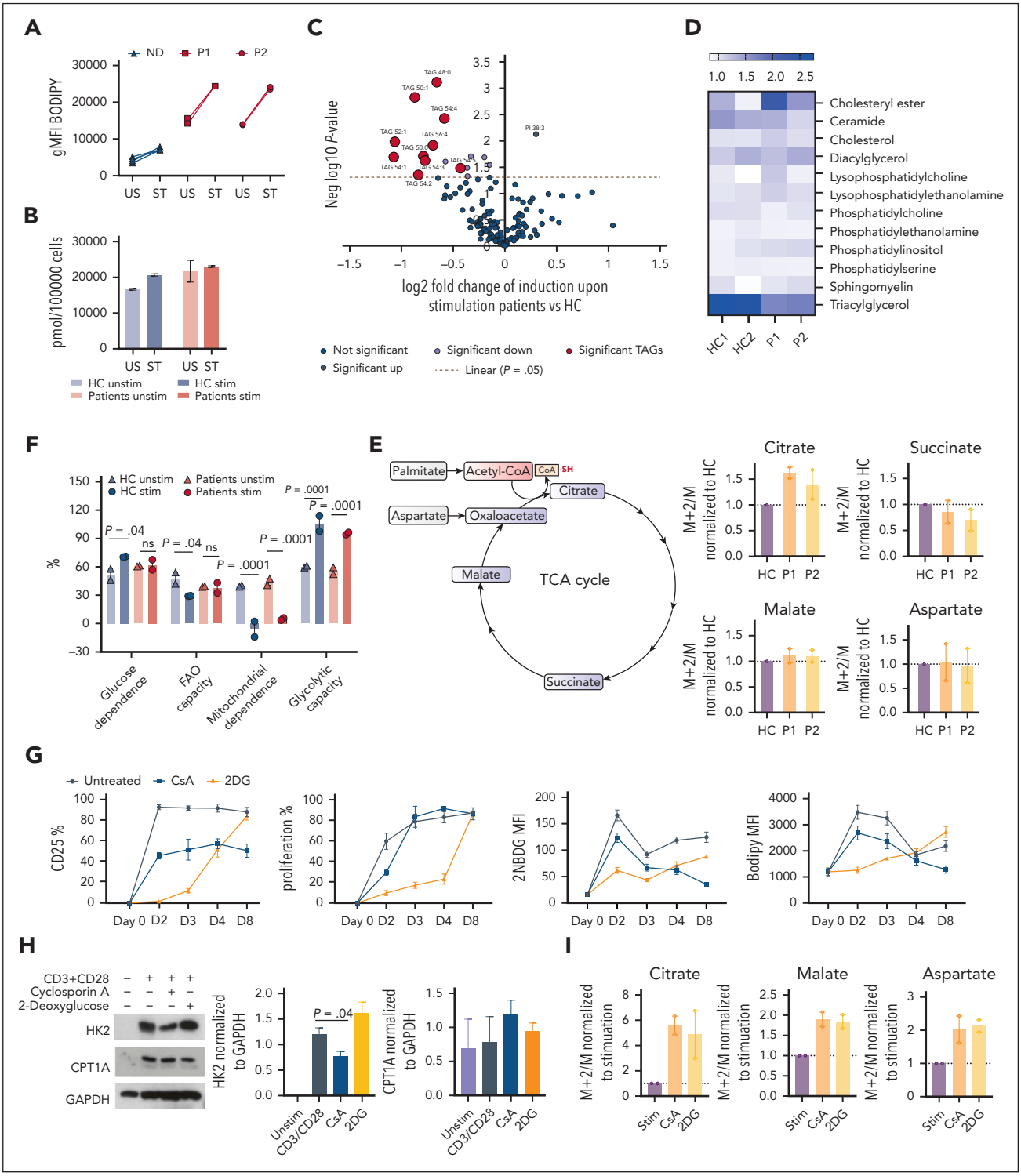

Figure 7. Shifted substrate preference toward FA oxidation in NFATc1-dysfunctional T cells. (A) Summary dot plot showing the lipid uptake of patient and HC T lymphoblasts after 24 hours of stimulation with soluble anti-CD3/CD28 antibodies using Bodipy FL C16 staining. (B) Bar graph showing the measured levels of total lipid species in HCs and patients with and without stimulation. (C) Volcano plot showing the $\log_2$ fold changes (x-axis) in lipid species upon stimulation in HCs vs patients. The y-axis represents the *P* values for $-\log_{10}$ of the measurements. Red full circles represent the TAG species, each significantly changed TAG species is indicated (statistics performed using *t* tests). (D) Heatmap showing fold changes in concentrations of different lipid species in patient and HC T lymphoblasts measured by mass spectrometry–based lipidomics after 24 hours of stimulation with soluble anti-CD3/CD28 antibodies. (E) Scheme depicting the TCA cycle and the TCA cycle intermediates that are detected in the current analysis. Summary graphs show the relative ^{13}C enrichment of TCA cycle intermediates in patient T lymphoblasts incubated in [U-$^{13}C_{16}$]palmitate, normalized to the HCs. (F) SCENITH analysis showing the metabolic alterations of patients (P1 and P2) and HCs (experiment 1: n = 4; experiment 2: n = 3) $CD8^+$ TEM population after CD3/CD28 bead stimulation. The experiment was performed twice and the plot shows the averaged results from each experimental replicate. The negative percentage values shown in the graph are inherent to the analysis of the assay. The calculation formulas are indicated in the supplemental Methods. Statistical analysis was performed using 2-way ANOVA with Bonferroni post hoc test to correct for multiple comparison. Sorted naïve T cells from HCs (n = 4) were treated with vehicle, CsA (300 nM), or 2-DG (1 μM), and stimulated them with Dynabeads coated with CD3 and CD28 antibodies. (G) Summary graphs showing the percentage of $CD8^+$ T cells with upregulated CD25 surface expression after

to 2-DG, although initially delayed with respect to the proliferation and activation (Figure 7G), managed to match responses of the stimulated, vehicle-treated cells by day 8. Importantly, this recovery in functional responses after the initial delay in 2-DG–treated cells was associated with a concomitant increase in lipid uptake (Figure 7G). Moreover, HK2 upregulation upon stimulation was normal in the 2-DG group whereas it was reduced in CsA-treated cells (Figure 7H), consistent with our patient data. Furthermore, both CsA and 2-DG treatment promoted [$^{13}C_{16}$]-palmitic acid incorporation into TCA cycle metabolites after TCR stimulation compared with stimulated, vehicle-treated control cells (Figure 7I). These data strongly suggest that glycolysis inhibition is sufficient to induce metabolic adaptations toward FAO.

NFATc1-mutant CD8$^+$ T cells possess a delayed, but not absent, responsiveness to stimulation, possibly associated with a subsequent adaptation toward FA use. Next, we tested whether CD8$^+$ T-cell effector functions could be improved through therapeutic metabolic reprogramming. We reasoned that early priming of cells toward FAO might diminish the delay in functional responses in CD8$^+$ T cells with ineffective glycolysis. We primed patient CD8$^+$ T cells with metformin and rosiglitazone, 2 therapies well documented for their effects on lipid catabolism.[42] Not only did CD8$^+$ T lymphoblasts from both patients increase IL-2 production with these treatments (supplemental Figure 14F), but treatment of patient PBMCs with metformin and rosiglizatone together with stimulation also led to improved proliferation, predominantly in rosiglitazone-treated patient CD8$^+$ T cells (supplemental Figure 14G-H). Taken together, these results demonstrate that NFATc1-mutant T cells may adapt to restricted glycolysis likely by shifting their substrate preference toward FAO after stimulation, thereby retaining some degree of functional capacity, which might be enhanced by metabolic priming as a potential therapeutic modulation.

Discussion

Here, we describe patients with inherited mutations in *NFATC1* that present with a novel combined immunodeficiency characterized by recurrent viral and bacterial infections, due to impaired T- and B-cell activation and proliferation. Through detailed profiling of these patients' immunophenotypes and comprehensive molecular experiments, we further authenticate the involvement of NFATc1 in establishing a cellular milieu that permits optimum glycolytic responses in T cells and reveal evidence of metabolic plasticity in the context of impaired glycolysis observed in patient T cells to remedy delayed effector responses. Lastly, through the metabolic priming of patient T cells, we provide preliminary proof-of-concept preclinical evidence for the therapeutic improvement of genetically defective T cells.

The role of the NFAT family of TFs, including the contribution of SOCE to the regulation of the NFAT axis on different phenotypes has been extensively characterized in mouse models. Recently, patients with LOF *NFATC2* mutations were reported and characterized by joint contractures, osteochondromas, and recurrent B-cell lymphoma.[43] Aspects of our patients' clinical presentations are shared by patients with NFATc2 deficiency including the aberrant T-cell functions. However, skeletal manifestations appear somewhat divergent. Although patients with mutated NFATc1 (patients P1 and P2) presented with scoliosis, likely reflecting an imbalance in bone remodeling processes for which NFATc1 has a well-documented role,[44] the joint contractures observed in patients with mutated NFATc2 points toward cartilage as the origin of the skeletal phenotype. A possible explanation for this is the expression profile differences between these proteins, with NFATc2 being more widely expressed compared with NFATc1, whose expression is more limited to the lymphoid/bone marrow compartment.

The phenotype of our patients is also reminiscent of ORAI/STIM1 deficiencies, the prototype diseases of defective SOCE,[6] which manifests with normal lymphocyte numbers, despite impairments in their activation and proliferation responses. Defective T- and B-cell activation in ORAI/STIM1 deficiency manifests as blunted NFAT activation and downstream effects on cytokine production.[6] Murine models revealed the essential role of NFATc1 in the regulation of multiple steps of both B- and T-cell development.[5,10,13,18,33] The defects in B-cell differentiation, activation, and class switch functions in our patients are consistent with those in mouse models, in which a prevailing theory suggests that a threshold level of NFATc1 expression is necessary for proper B-cell development. The relatively milder phenotype observed in P2 might be because of the higher protein expression. However, larger cohorts of patients with defective NFATc1 will be required to address such a relationship between NFATc1 protein expression and severity of clinical presentations and/or impaired B-cell functioning. SOCE also controls transcriptional networks that determine the differentiation of CD4$^+$ T cells into TfHs and Tregs, evidenced by patients with deficient STIM1 who develop autoimmune thrombocytopenia and hemolytic anemia. Although autoimmunity is also a defining feature in *Nfatc1*$^{-/-}$ mice, no such clinical evidence for autoimmunity in our patients was observed despite having fewer circulating Tregs. Nonetheless, additional patient cohorts will be needed to clarify whether any causal link between NFATc1 dysfunction and autoimmunity exists.

Despite the substantial data generated using murine models, mechanisms by which NFAT controls the switch of T cells from

Figure 7 (continued) stimulation with CD3/CD28 Dynabeads and percentage of proliferation by measuring dilution of the VPD450 in CD8$^+$ T cells at basal state (day 0), and on days 2, 3, 4, and 8 after stimulation in vehicle-, CsA-, or 2-DG–treated cells. Summary graphs showing the gMFI of 2-NBDG and Bodipy FL16 in CD8$^+$ T cells after stimulation with CD3/CD28 beads measured via flow cytometry at basal state (unstimulated), and on days 2, 3, 4, and 8 after stimulation. (H) (Left) Immunoblot showing the protein expression levels of HK2, CPT1a, and GAPDH. (Right) Graphs showing the quantification of the western blots averaged from 3 independent experiments displaying the expressions of HK2 and CPT1a on HC naïve T cells harvested on day 4 after stimulation with Dynabeads. (I) Summary graphs show the relative ^{13}C enrichment of TCA cycle intermediates (citrate, malate, and aspartate) in HC T cells stimulated with Dynabeads (for 4 days) and treated with CsA, 2-DG, or vehicle, incubated in [U-$^{13}C_{16}$] palmitate and normalized to the vehicle treatment. All data are mean ± SEM. Statistics performed using one-way ANOVA with post hoc Bonferroni correction if not stated otherwise.

the quiescent to proliferative state have remained elusive. A proposed mechanism involves transcriptional regulation of *IL2*[45,46]; however, results from animal studies remain discordant.[7,39] Although in some animal studies, IL-2 partially rescued the T-cell dysfunction,[10] additional IL-2 did not restore apoptosis in our patient cells and only slightly improved TCR-induced proliferation in patients with ORAI/STIM1 deficiency.[39] Our finding of impaired glycolytic capacity in NFATc1-mutant T cells is consistent with that in Nfatc1- and Stim1-deficient murine T cells,[10,36] attesting to the essential role of the SOCE/NFAT axis in regulating glycolytic capacity and subsequent T-cell proliferation. However, the functional responses were delayed rather than absent in the NFATc1 mutant T cells, prompting us to question whether this delay corresponded to cells adapting to the impaired glycolytic capacity by enhancing alternative metabolic preferences. Indeed, fluxomic experiments helped confirm that palmitate-derived carbons were incorporated more readily into the TCA cycle in NFATc1-mutant lymphocytes than in HC lymphocytes, suggesting an increased use of FAO.[47]

Because the initial engagement of glycolysis appeared most relevant in naïve cells in terms of coordinating initial effector responses,[1,2] we assessed whether naïve $CD8^+$ T cells would similarly modify their metabolic preference toward FAO upon the inhibition of glycolysis induced with the use of 2-DG. 2-DG inhibited initial proliferation and activation responses in naïve $CD8^+$ T cells from HCs, consistent with that reported in literature[1,2] and mirrored the delayed effector responses in our patient T cells. Similar to our patient cells, TCA cycle incorporation of ^{13}C-labeled palmitate-derived carbons were higher in TCR-activated T cells exposed to 2-DG compared with those exposed to vehicle, indicating a greater reliance on FAs as a substrate. Importantly, markers of increased lipid uptake and incorporation into the TCA cycle induced by 2-DG preceded the recovery of functional responses to levels of the vehicle-treated cells. Thus, although observations that proliferation and survival of T cells can persist in vitro when glycolysis is ablated have been reported,[47] to the best of our knowledge, this is the first evidence of metabolic adaptation established in the setting of an IEI.

Not addressed specifically in this study are the underlying stimuli and mechanisms for the shifted preference toward FAO in NFATc1-mutant T cells. Thus, although NFATc1-mutant T cells have altered HK2 expression after stimulation, whether this is responsible for the glycolytic defect in patient T cells is uncertain, particularly given the data from murine *Hk2*$^{-/-}$ T cells, which retain intact glycolysis and are grossly immunologically normal.[48] Kaymak et al[49] revealed that shifted fuel preferences in T cells could occur in the absence of major differences in global transcriptional changes of metabolic programs,[49] suggesting that metabolite concentrations per se exert a greater influence on the immediate and dynamic control of metabolic fuel selection.[50] We focused our attention on lipids for which associated metabolic pathways are sensitive to changes in glucose use dynamics.[51-53] NFATc1-defective T cells had attenuated increase in the triacylglycerol (TAG) pool after stimulation, despite markers of FA uptake being higher, suggesting increased use, consistent with the elevated CPT1a levels and palmitate-derived carbon incorporation into the TCA cycle. However, whether increased FAO is engaged to alleviate an energetic deficit or for some other compensation is unknown. The pentose phosphate pathway is essential for T-cell functions, particularly for proliferative purposes in which glucose gets consumed to generate biosynthetic precursors for DNA and RNA synthesis as well as reduced NAD phosphate, which is required for de novo FA and cholesterol biosynthesis.[54] Thus, it is possible that FAO is engaged in response to impaired glucose–pentose phosphate pathway flux in order to sustain cytosolic reduced NAD phosphate pools.[53,55] Inadvertently, such an adaptation would serve not only to sustain proliferative capacity but also act to promote survival by supporting defenses against oxidative stress.[53,55-57] Additional advanced substrate-tracing experiments would be required to evaluate crossmetabolic pathway regulation and engagement as well as shifted use of other nonconventional substrates such as amino acids and lactate by NFATc1-mutant T cells.

Our observations that the contribution of FA to oxidative metabolism is higher in NFATc1-mutant T cells than in WT NFATc1 T cells and that 2-DG treatment promotes a metabolic shift toward FA use, led us to consider the therapeutic priming of patient T cells in order to promote FAO and evaluate whether this might improve T effector–cell functionality. We tested this hypothesis using metformin and rosiglitazone, substances with well-characterized effects on FAO.[58-61] These drugs were able to induce a modest, albeit reproducible, increase in IL-2 expression in patient T lymphocytes expanded in vitro. Experiments performed on limited patient material restricted us from making firm conclusions about these data regarding their significance or clinical relevance and obtaining in vivo evidence from patients (eg, in the scope of a clinical trial) is outside the scope of this study. Nonetheless, a growing body of literature supports the premise that increasing FAO can improve the development and quality of $CD8^+$ T cells,[54] suggesting metabolic priming as a promising line of inquiry. Additional experiments are required to elucidate how IL-2 production is improved by these compounds in NFATc1-defective T cells. It would also be interesting to assess whether murine *Nfatc1*$^{-/-}$ T cells similarly adapt to restricted glycolysis by increasing FA use and whether their immune-dysregulated features can be improved with pharmacological approaches that target metabolic pathways and to dissect the responsible underlying cellular mechanisms.

Collectively, we report functional NFATC1 deficiency as a novel IEI and provide evidence that NFATc1-mutant T cells adapt to impairments in their glycolytic capacity by increasing their reliance on FA use, showcasing the phenomena of metabolic plasticity in a transcriptionally defective genetic landscape. The extent to which other IEIs can be classified by specific metabolic signatures irrespective of their genetic etiology and/or sensitivity to therapies that target metabolic pathways warrants further research.

Acknowledgments

The authors thank the patients and their family members for their participation in our study. The authors also thank the Biomedical Sequencing Facility for their WES, RNA sequencing, and ATACseq service, and The Bergthaler Lab for the use of Seahorse XFe 96 machine at the CeMM Research Center of Molecular Medicine) of the Austrian Academy of Sciences. The authors thank Daniela Reil and the Molecular Discovery Platform at CeMM for technical support with metabolomics analyses. The authors thank MUW Core Facility Flow Cytometry Unit and Andreas Spittler for their help in imaging flow cytometry. The authors

thank Tatjana Hirschmugl for the illustration in the visual abstract. The authors thank Wolfgang Weninger for providing the infrastructure required for processing the single-cell RNA-sequencing libraries and relevant discussions.

This study has been supported by the European Research Council Consolidator Grant iDysChart (ERC grant agreement number: 820074). S.B. has been supported by The Scientific and Technological Research Council of Turkey (318S202). C.H. and F.H. are supported by funding from the Alex's Lemonade Stand Foundation for Childhood Cancer (20-17258). M.J.K. has been supported by an FWF Lise Meitner Postdoctoral Fellowship (M2013). J.B. has been supported by a DOC Fellowship of the Austrian Academy of Sciences (25590). C.v.d.W. has been supported by a Postdoctoral Fellowship of the PT Engelhorn Foundation. B.R. has been supported by PhD fellowship from the FFG (879254).

Authorship

Contribution: S.K.B. performed most of the experiments on patient material and analyzed and interpreted the patient and experimental data; S.K.B., S.G., J.B., and T.S. performed the biochemical experiments, with help from V.H.; S.K.B. supervised S.G.; M.J.K. and S.K.B. planned the metabolism experiments and performed and analyzed the data, with technical assistance from S.G.; M.S. analyzed the RNA-sequencing data under supervision of C.B.; P.R. analyzed the RNA-sequencing and ATACseq data; C.H. analyzed the single-cell RNA-sequencing data and rerun the pipeline for the ATACseq under the supervision of F.H.; R.J.H. identified the variant, and performed the WES, ATACseq, and RNA-sequencing preparation; A.F. performed the segregation analysis and protein conservation analysis, and quantitative polymerase chain reaction experiments; I. Chowdhury and M.V. gave intellectual input; J.B. assisted in imaging analysis and provided critical intellectual input; S.K.B. and B.R. prepared samples and interpreted the single-cell RNA-sequencing results; B.R. performed the B-cell activation, proliferation, and class switch experiments; Y.M. assisted with the tissue culture of T cells and imaging experiments; C.v.d.W. repeated western blotting for coimmunoprecipitation experiments, assisted in the data analysis of hexokinase assay, provided intellectual input, and helped with manuscript preparation; S.Z. assisted in tissue culture of B cells and transfection of EBV B cells; M.T. assisted in the B-cell class switch assays; A.B. reran the pipeline for RNA-sequencing experiments and replotted the gene set enrichment analysis graphs; L.E.S. performed single-cell RNA sequencing under the supervision of M.F.; S.B. recruited patients in Turkey and supervised patient follow-ups; N.K., R.B., S.B.E., E.K.-A., and A.O. performed patient follow-ups and assisted in the collection of medical data; R.J.A. provided the necessary material, protocols, and consultancy for SCENITH experiments; E.S. provided critical intellectual input in interpretation of the NFAT cellular assays; L.D. provided protocols and consultancy for the T-cell functional experiments (T-cell expansion, imaging, and degranulation); J.T.H. performed mass spectrometry for metabolomics, lipidomics, and fluxomics and performed the initial data analysis; S.K.B., M.K., I. Castanon, and K.B. wrote the manuscript with input from all coauthors; and K.B. conceptualized and coordinated the study, provided laboratory resources, and took overall responsibility of the study.

Conflict-of-interest disclosure: The authors declare no competing financial interests.

The current affiliation for M.T. is Global Drug Safety Research and Evaluation, Takeda Pharmaceuticals USA, Inc, Cambridge, MA.

ORCID profiles: S.K.B., 0000-0002-3718-5323; S.G., 0000-0001-8735-8491; J.B., 0009-0003-6458-3903; P.R., 0000-0002-7335-8324; C.H., 0000-0001-6365-8254; T.S., 0000-0001-8030-1257; N.K., 0000-0001-5432-4076; C.v.d.W., 0000-0002-4715-6016; A.F., 0000-0001-6641-4001; M.S., 0000-0003-2975-8969; S.Z., 0000-0002-9015-4446; V.H., 0000-0003-4476-6748; M.T., 0000-0002-3016-0430; A.B., 0000-0003-4532-9865; R.B., 0000-0002-1044-2174; S.B.E., 0000-0003-0561-3343; L.E.S., 0000-0003-2273-7655; I. Chowdhury, 0000-0002-0360-6951; M.V., 0000-0002-1340-9732; R.J.A., 0000-0001-9785-3883; M.F., 0000-0003-0698-2992; A.O., 0000-0002-9065-1901; C.B., 0000-0001-6091-3088; F.H., 0000-0003-2452-4784; J.T.H., 0000-0002-2286-4956; S.B., 0000-0002-4730-9422; K.B., 0000-0001-8387-9185.

Correspondence: Kaan Boztug, St. Anna Children's Cancer Research Institute, Zimmermannplatz 10, A-1090 Vienna, Austria; email: kaan.boztug@ccri.at.

Footnotes

Submitted 6 September 2022; accepted 17 May 2023; prepublished online on *Blood* First Edition 30 May 2023. https://doi.org/10.1182/blood.2022018303.

*S.B. and K.B. contributed equally to this study.

Raw sequencing reads are deposited in the European Genome-Phenome Archive (accession numbers EGAS00001007270 [RNAseq], EGAS00001007271 [scRNAseq], EGAS00001007273 [ATACseq]). These data are available via controlled access to safeguard patient privacy.

R code used for the analysis of single-cell RNA-sequencing data is available on GitHub at https://github.com/cancerbits/nfatc1.

Raw data from liquid chromatography mass spectrometry are available at https://www.ebi.ac.uk/metabolights/MTBLS7925.

The online version of this article contains a data supplement.

The publication costs of this article were defrayed in part by page charge payment. Therefore, and solely to indicate this fact, this article is hereby marked "advertisement" in accordance with 18 USC section 1734.

REFERENCES

1. Geltink RIK, Kyle RL, Pearce EL. Unraveling the complex interplay between T cell metabolism and function. *Annu Rev Immunol*. 2018;36:461-488.
2. Buck MD, Sowell RT, Kaech SM, Pearce EL. Metabolic instruction of immunity. *Cell*. 2017;169(4):570-586.
3. Hermann-Kleiter N, Baier G. NFAT pulls the strings during CD4+ T helper cell effector functions. *Blood*. 2010;115(15):2989-2997.
4. Hogan PG. Calcium-NFAT transcriptional signalling in T cell activation and T cell exhaustion. *Cell Calcium*. 2017;63:66-69.
5. Vaeth M, Feske S. NFAT control of immune function: new frontiers for an abiding trooper. *F1000Res*. 2018;7:260.
6. Lacruz RS, Feske S. Diseases caused by mutations in ORAI1 and STIM1. *Ann N Y Acad Sci*. 2015;1356(1):45-79.
7. Vaeth M, Kahlfuss S, Feske S. CRAC channels and calcium signaling in T cell-mediated immunity. *Trends Immunol*. 2020;41(10):878-901.
8. Martinez GJ, Pereira RM, Aijo T, et al. The transcription factor NFAT promotes exhaustion of activated CD8(+) T cells. *Immunity*. 2015;42(2):265-278.
9. Baur J, Otto C, Steger U, et al. The transcription factor NFATc1 supports the rejection of heterotopic heart sllografts. *Front Immunol*. 2018;9:1338.
10. Klein-Hessling S, Muhammad K, Klein M, et al. NFATc1 controls the cytotoxicity of CD8(+) T cells. *Nat Commun*. 2017;8(1):511.
11. Shahin T, Kuehn HS, Shoeb MR, et al. Germline biallelic mutation affecting the transcription factor Helios causes pleiotropic defects of immunity. *Sci Immunol*. 2021;6(65):eabe3981.
12. Martinez GJ, Hu JK, Pereira RM, et al. Cutting edge: NFAT transcription factors promote the

generation of follicular helper T cells in response to acute viral infection. *J Immunol*. 2016;196(5):2015-2019.

13. Klein-Hessling S, Rudolf R, Muhammad K, et al. A threshold level of NFATc1 activity facilitates thymocyte differentiation and opposes notch-driven leukaemia development. *Nat Commun*. 2016;7:11841.

14. Rudolf R, Busch R, Patra AK, et al. Architecture and expression of the nfatc1 gene in lymphocytes. *Front Immunol*. 2014; 5:21.

15. Yoshida H, Nishina H, Takimoto H, et al. The transcription factor NF-ATc1 regulates lymphocyte proliferation and Th2 cytokine production. *Immunity*. 1998;8(1):115-124.

16. Pachulec E, Neitzke-Montinelli V, Viola JP. NFAT2 regulates generation of innate-like CD8(+) T lymphocytes and CD8(+) T lymphocytes responses. *Front Immunol*. 2016;7:411.

17. Guram K, Kim SS, Wu V, et al. A threshold model for T-cell activation in the era of checkpoint blockade immunotherapy. *Front Immunol*. 2019;10:491.

18. Bhattacharyya S, Deb J, Patra AK, et al. NFATc1 affects mouse splenic B cell function by controlling the calcineurin–NFAT signaling network. *J Exp Med*. 2011;208(4):823-839.

19. Hao Y, Hao S, Andersen-Nissen E, et al. Integrated analysis of multimodal single-cell data. *Cell*. 2021;184(13):3573-3587.e29.

20. Huang XP, Karpiak J, Kroeze WK, et al. Allosteric ligands for the pharmacologically dark receptors GPR68 and GPR65. *Nature*. 2015;527(7579):477-483.

21. Mehta HH, Xiao J, Ramirez R, et al. Metabolomic profile of diet-induced obesity mice in response to humanin and small humanin-like peptide 2 treatment. *Metabolomics*. 2019;15(6):88.

22. Sasako T, Ohsugi M, Kubota N, et al. Hepatic Sdf2l1 controls feeding-induced ER stress and regulates metabolism. *Nat Commun*. 2019;10(1):947.

23. Yen K, Lee C, Mehta H, Cohen P. The emerging role of the mitochondrial-derived peptide humanin in stress resistance. *J Mol Endocrinol*. 2013;50(1):R11-R19.

24. Femel J, van Hooren L, Herre M, et al. Vaccination against galectin-1 promotes cytotoxic T-cell infiltration in melanoma and reduces tumor burden. *Cancer Immunol Immunother*. 2022;71(8):2029-2040.

25. Seo W, Jerin C, Nishikawa H. Transcriptional regulatory network for the establishment of CD8(+) T cell exhaustion. *Exp Mol Med*. 2021;53(2):202-209.

26. Zaiss DM, van Loosdregt J, Gorlani A, et al. Amphiregulin enhances regulatory T cell-suppressive function via the epidermal growth factor receptor. *Immunity*. 2013;38(2): 275-284.

27. Kallies A, Hawkins ED, Belz GT, et al. Transcriptional repressor Blimp-1 is essential for T cell homeostasis and self-tolerance. *Nat Immunol*. 2006;7(5):466-474.

28. Raghu D, Xue HH, Mielke LA. Control of lymphocyte fate, infection, and tumor immunity by TCF-1. *Trends Immunol*. 2019; 40(12):1149-1162.

29. Seo H, Chen J, Gonzalez-Avalos E, et al. TOX and TOX2 transcription factors cooperate with NR4A transcription factors to impose CD8(+) T cell exhaustion. *Proc Natl Acad Sci U S A*. 2019;116(25):12410-12415.

30. Federico A, Monti S. hypeR: an R package for geneset enrichment workflows. *Bioinformatics*. 2020;36(4):1307-1308.

31. Heikamp EB, Patel CH, Collins S, et al. The AGC kinase SGK1 regulates TH1 and TH2 differentiation downstream of the mTORC2 complex. *Nat Immunol*. 2014;15(5):457-464.

32. Liu Z, Han M, Ding K, Fu R. The role of Pim kinase in immunomodulation. *Am J Cancer Res*. 2020;10(12):4085-4097.

33. Giampaolo S, Wojcik G, Klein-Hessling S, Serfling E, Patra AK. B cell development is critically dependent on NFATc1 activity. *Cell Mol Immunol*. 2019;16(5):508-520.

34. Pham LV, Tamayo AT, Li C, Bueso-Ramos C, Ford RJ. An epigenetic chromatin remodeling role for NFATc1 in transcriptional regulation of growth and survival genes in diffuse large B-cell lymphomas. *Blood*. 2010; 116(19):3899-3906.

35. Love MI, Huber W, Anders S. Moderated estimation of fold change and dispersion for RNA-seq data with DESeq2. *Genome Biol*. 2014;15(12):550.

36. Miller M. The importance of being flexible: the case of basic region leucine zipper transcriptional regulators. *Curr Protein Pept Sci*. 2009;10(3):244-269.

37. Schraml BU, Hildner K, Ise W, et al. The AP-1 transcription factor Batf controls T(H)17 differentiation. *Nature*. 2009;460(7253): 405-409.

38. Subramanian A, Tamayo P, Mootha VK, et al. Gene set enrichment analysis: a knowledge-based approach for interpreting genome-wide expression profiles. *Proc Natl Acad Sci U S A*. 2005;102(43):15545-15550.

39. Vaeth M, Maus M, Klein-Hessling S, et al. Store-operated Ca(2+) entry controls clonal expansion of T cells through metabolic reprogramming. *Immunity*. 2017;47(4): 664-679.e6.

40. Arguello RJ, Combes AJ, Char R, et al. SCENITH: a flow cytometry-based method to functionally profile energy metabolism with single-cell resolution. *Cell Metab*. 2020;32(6): 1063-1075.e7.

41. Wong GK, Goldacker S, Winterhalter C, et al. Outcomes of splenectomy in patients with common variable immunodeficiency (CVID): a survey of 45 patients. Research support, non-U.S. gov't. *Clin Exp Immunol*. 2013;172(1): 63-72.

42. Palsson-McDermott EM, O'Neill LAJ. Targeting immunometabolism as an anti-inflammatory strategy. *Cell Res*. 2020;30(4): 300-314.

43. Sharma M, Fu MP, Lu HY, et al. Human complete NFAT1 deficiency causes a triad of joint contractures, osteochondromas, and B-cell malignancy. *Blood*. 2022;140(17): 1858-1874.

44. Sitara D, Aliprantis AO. Transcriptional regulation of bone and joint remodeling by NFAT. *Immunol Rev*. 2010;233(1):286-300.

45. Nadeau S, Martins GA. Conserved and unique functions of blimp1 in immune cells. *Front Immunol*. 2021;12:805260.

46. Xiao Y, Qureischi M, Dietz L, et al. Lack of NFATc1 SUMOylation prevents autoimmunity and alloreactivity. *J Exp Med*. 2021;218(1):e20181853.

47. Chang CH, Curtis JD, Maggi LB Jr, et al. Posttranscriptional control of T cell effector function by aerobic glycolysis. *Cell*. 2013; 153(6):1239-1251.

48. Mehta MM, Weinberg SE, Steinert EM, et al. Hexokinase 2 is dispensable for T cell-dependent immunity. *Cancer Metab*. 2018; 6:10.

49. Kaymak I, Luda KM, Duimstra LR, et al. Carbon source availability drives nutrient utilization in CD8(+) T cells. *Cell Metab*. 2022; 34(9):1298-1311.e6.

50. Hackett SR, Zanotelli VR, Xu W, et al. Systems-level analysis of mechanisms regulating yeast metabolic flux. *Science*. 2016;354(6311):aaf2786.

51. Pearce EL, Walsh MC, Cejas PJ, et al. Enhancing CD8 T-cell memory by modulating fatty acid metabolism. *Nature*. 2009; 460(7251):103-107.

52. Raud B, McGuire PJ, Jones RG, Sparwasser T, Berod L. Fatty acid metabolism in CD8(+) T cell memory: challenging current concepts. *Immunol Rev*. 2018;283(1):213-231.

53. Jeon SM, Chandel NS, Hay N. AMPK regulates NADPH homeostasis to promote tumour cell survival during energy stress. *Nature*. 2012;485(7400):661-665.

54. Klein Geltink RI, Edwards-Hicks J, Apostolova P, et al. Metabolic conditioning of CD8(+) effector T cells for adoptive cell therapy. *Nat Metab*. 2020;2(8):703-716.

55. Carracedo A, Cantley LC, Pandolfi PP. Cancer metabolism: fatty acid oxidation in the limelight. *Nat Rev Cancer*. 2013;13(4): 227-232.

56. Carracedo A, Weiss D, Leliaert AK, et al. A metabolic prosurvival role for PML in breast cancer. *J Clin Invest*. 2012;122(9):3088-3100.

57. Samudio I, Harmancey R, Fiegl M, et al. Pharmacologic inhibition of fatty acid oxidation sensitizes human leukemia cells to apoptosis induction. *J Clin Invest*. 2010; 120(1):142-156.

58. Nicoli F, Cabral-Piccin MP, Papagno L, et al. Altered basal lipid metabolism underlies the functional impairment of naive CD8(+) T cells in elderly humans. *J Immunol*. 2022;208(3): 562-570.

59. Xu L, Ma X, Verma N, et al. PPARgamma agonists delay age-associated metabolic disease and extend longevity. *Aging Cell*. 2020;19(11):e13267.

60. Renner K, Geiselhoringer AL, Fante M, et al. Metabolic plasticity of human T cells: Preserved cytokine production under glucose deprivation or mitochondrial restriction, but 2-deoxy-glucose affects effector functions. *Eur J Immunol*. 2015;45(9):2504-2516.

61. Zhou J, Massey S, Story D, Li L. Metformin: an old drug with new applications. *Int J Mol Sci*. 2018;19(10):2863.